Modeling and Numerical Analysis of Dead-Core Phenomena in Chemical Reactor Engineering

by

Al-Tarazi Assaubay

Submitted to the Department of Mathematics
in partial fulfillment of the requirements for the degree of

Master of Science in Applied Mathematics

at the

NAZARBAYEV UNIVERSITY

May 2021

Author .....
Department of Mathematics

Certified by .....
Piotr Skrzypacz
Assistant Professor
Thesis Supervisor

Accepted by .....
Daniel Pugh
Dean, School of Sciences and Humanities

Modeling and Numerical Analysis of Dead-Core Phenomena in Chemical Reactor Engineering

by

Al-Tarazi Assaubay

Submitted to the Department of Mathematics
on , in partial fulfillment of the
requirements for the degree of
Master of Science in Applied Mathematics

Abstract

Diffusion-reaction processes in chemical reactors are often modelled by differential equations of diffusion-reaction type that describe the change in time and space of concentrations of chemical species. In this work, dead-core phenomena, i.e. depleting of chemical species due to the strong catalytic reactions, are studied analytically and numerically for single reactions with power-law kinetics of fractional order. In the first part of this work, dead-core phenomena are presented for 1-D diffusion-reaction problems for catalytic pellets. The point-wise convergence of the classical solution of non-stationary problems to the solution of the steady-state limit is shown analytically which constitutes the basis for the construction of an appropriate time-marching scheme to solve numerically stationary diffusion-reaction problems. In the second part of this work, 2-D reactor problems are studied. The spatial discretization is based on Finite Element Method (FEM) where the modified Crank-Nicolson method is used for the time-marching approach. The developed numerical scheme is implemented in *MATLAB* using Partial Differential Toolbox (PDE Toolbox). The simulation results confirm the theoretical predictions. Also, the phenomenon of dead-cores at the boundary is studied numerically for the model of chemical reactor with a catalytic membrane.

Thesis Supervisor: Piotr Skrzypacz
Title: Assistant Professor

Acknowledgements

I want to express gratitude to my supervisor, Professor Piotr Skrzypacz for a huge support. Our fruitful discussions led to immediate progress. I also want to thank my family and friends for a support during my hard work.

Contents

Chapter 1

Introduction

1.1 Mathematical model

Chemical reactor is a closed volume in which a chemical reaction occurs, as stated in [11, Section 19, p. 4]. Derivation of the differential equation for the chemical reactor is adapted from [9], the only difference is that we assume that the temperature is constant. In the following, the single chemical reaction

$$A \to B \tag{1.1}$$

is considered. Modeling of a chemical reactor that will be presented below is based on [10, p. 2]. Let Ω be a domain for a chemical reactor and consider an arbitrary subset $\tilde{\Omega} \subset \Omega$, in which there is defined a concentration $u(x,t)$ of substance A. The rate of change of the total concentration in $\tilde{\Omega}$ is given by

$$\partial_t \int_{\tilde{\Omega}} u(x,t)dx\,. \tag{1.2}$$

If (1.2) is not zero, then, due to conservation of mass there could be two possible cases: either decrease of concentration or increase, or both. In the case of chemical reactor they are

$$-\int_{\partial\tilde{\Omega}} J(x,t)\nu(x)ds, \qquad \int_{\tilde{\Omega}} R(x,t)dx, \tag{1.3}$$

where the first one is a flux of the component through the walls of reactor was adapted from [10] and the second expression is total reaction rate in $\tilde{\Omega}$. In the expression for the flux of the component $J(x,t)$ if the flux density, and $\nu(x)$ is outer normal. Then, the conservation of mass reads as follows

$$\partial_t \int_{\tilde{\Omega}} u(x,t)dx = -\int_{\partial\tilde{\Omega}} J(x,t)\nu(x)ds - \int_{\tilde{\Omega}} R(x,t)dx, \tag{1.4}$$

where in front of total reaction rate we have minus sign, because reaction uses substance A, i.e. concentration of substance A decreases, resulting in a negative rate of change. Using the integral theorem of Gauss from [10, eq. 2.3] the above equation (1.4) can be rewritten as

$$\int_{\tilde{\Omega}} \partial_t u(x,t) + \nabla J(x,t) + R(x,t)dx = 0, \tag{1.5}$$

and since $\tilde{\Omega}$ is arbitrary subset, the following holds true

$$\partial_t u(x,t) + \nabla J(x,t) + R(x,t) = 0\,. \tag{1.6}$$

Now, using Fick's law (see [10]): $J(x,t) = -K\nabla u$, where $K > 0$ is molecular diffusivity, (1.6) becomes

$$u_t - K\Delta u + R(x,t) = 0, \tag{1.7}$$

since $\nabla(\nabla u) = \Delta u$, and $u_t = \partial_t u$. In this thesis, the reaction kinetics is of power-law type with fraction exponent $p \in (0,1)$

$$R(x,t) = \alpha[u]_+^p(x,t), \tag{1.8}$$

where α is reaction rate constant, and $[u]_+$ denotes the non-negative part of u, namely:

$$[u]_+ = \begin{cases} u, & \text{if } u \geq 0, \\ 0, & \text{if } u < 0. \end{cases}$$

Such types of reaction kinetics were used in the following studies [16], [15], [4], [18], [2]. Examples of reactions with fractional exponent $p \in (0,1)$ are hydrogenation of propylene (see [19]) and combustion of methane (see [17]).

Thus, substituting (1.8) into (1.7) results in

$$u_t - K\Delta u + \alpha[u]_+^p = 0. \tag{1.9}$$

In order to nondimensionalize the equation, the following variables and parameters will be introduced

$$\hat{t} = L^2\frac{t}{K}, \qquad \phi = \sqrt{\frac{L^2\alpha u_{ref}^{p-1}}{K}}, \qquad \hat{u} = \frac{u}{u_{ref}}, \tag{1.10}$$

where L stands for the reference reactor length and u_{ref} is the reference concentration. Hence, the diffusion reaction problem reads as follows

$$\hat{u}_{\hat{t}} - \Delta\hat{u} + \phi^2[\hat{u}]_+^p = 0, \tag{1.11}$$

which, for simplicity, will be written as

$$u_t - \Delta u + \phi^2[u]_+^p = 0\,. \tag{1.12}$$

Then, the corresponding steady-state problem is

$$-\Delta u + \phi^2[u]_+^p = 0. \tag{1.13}$$

Many recent articles, such as [1], [16], [15], studied chemical reactors using the model (1.13). By applying different boundary conditions, we can create different scenarios of possible reactor configurations. One of the most interesting phenomena that can occur in the chemical reactor engineering is the so-called dead-core (also called dead-zone). Dead-core is a space inside the reactor where the substance is already completely

vanished, so that there is no reaction. Mathematically it can be defined as a set

$$\{x \in \Omega \,:\, u(x) = 0\}, \tag{1.14}$$

where Ω represents the bounded reactor domain. As stated in [15], the presence dead-cores leads to inefficient use of catalyst material. In other words, catalytic reaction might terminate due to the occurrence of dead-core, which means that expensive catalysts are simply wasted. Thus, it is crucial to identify dead-cores, to find out if it is possible to decrease the size of the dead-core, or to avoid it at all. However, before dealing with multi-dimensional problems, the dead-core phenomena will be illustrated in the next section for a simple one-dimensional model.

1.2 Dead-core phenomenon in 1-d model problem

The dead-core phenomenon can be illustrated by considering the one-dimensional model (1.13) with simple Dirichlet boundary conditions

$$\begin{aligned} -u'' + \phi^2 [u]_+^p = 0, \quad & \text{in } (0,1), \\ u = 1, \quad & \text{on } \{0,1\}. \end{aligned} \tag{1.15}$$

Let us assume that the solution $u(x)$ is of the following form $u(x) = (Ax+B)^C$. Then, substituting into the equation, we obtain that

$$A^2 C(C-1)(Ax+B)^{C-2} = \phi^2 (Ax+B)_+^{Cp}\,.$$

Assuming $Ax + B \geq 0$, we have that

$$\begin{aligned} C &= \frac{2}{1-p}, \\ A &= \pm\sqrt{\frac{\phi^2(1-p)^2}{2(1+p)}}\,. \end{aligned}$$

For convenience, let $A = \pm\frac{1}{a}$. Thus,

$$a = \sqrt{\frac{2(1+p)}{(1-p)^2\phi^2}}\,.$$

Then, we discuss the solution $u(x)$ in the three following cases.

Case 1

$$\begin{aligned}
u(x) &= \Big(\frac{x}{a} + B\Big)^{\frac{2}{1-p}}, \quad \text{using boundary condition at x=1, we have} \\
u(1) &= \Big(\frac{1}{a} + B\Big)^{\frac{2}{1-p}} = 1, \quad \text{thus } \frac{1}{a} + B = 1, \quad \text{and } B = 1 - \frac{1}{a}, \\
u(x) &= \Big(\frac{x}{a} + 1 - \frac{1}{a}\Big)^{\frac{2}{1-p}}, \\
u(x) &= (1 - \frac{1-x}{a})^{\frac{2}{1-p}}.
\end{aligned}$$

Since we assumed that $Ax + B > 0$, the condition that has to be satisfied is the following

$$1 - \frac{1-x}{a} > 0, \quad \text{then } 1 - a < x \leq 1.$$

Case 2

$$\begin{aligned}
u(x) &= \Big(-\frac{x}{a} + B\Big)^{\frac{2}{1-p}}, \quad \text{using boundary condition at x=0, we have} \\
u(0) &= B^{\frac{2}{1-p}} = 1, \quad \text{thus } B = 1, \\
u(x) &= \Big(-\frac{x}{a} + 1\Big).
\end{aligned}$$

As before, because of the condition that $Ax + B > 0$, the above solution is true for

$$0 \leq x < a.$$

Case 3

$$\begin{aligned}
u(x) &= 0, \\
\pm\frac{x}{a} + b &= 0.
\end{aligned}$$

The above make sense only for a, such that $a \leq x \leq 1-a$, since this is a possible interval for x such that $u(x) = 0$. Note that all three cases exist if $a \leq 1-a$, thus we have $a \leq 1/2$. Therefore, the exact dead-core solution is given by

$$u(x) = \begin{cases} \left(1 - \frac{x}{a}\right)^{\frac{2}{1-p}} & \text{for } 0 \leq x < a, \\ 0 & \text{for } a \leq x \leq 1-a, \\ \left(1 - \frac{1-x}{a}\right)^{\frac{2}{1-p}} & \text{for } 1-a < x \leq 1. \end{cases}$$

Substituting back expression for a, the necessary condition for the above analytical solution is obtained:

$$\phi^2 \geq \frac{8(1+p)}{(1-p)^2}. \tag{1.16}$$

If

$$\phi^2 < \frac{8(1+p)}{(1-p)^2},$$

then the solution can not be expressed by using elementary functions and numerical schemes have to be employed. In other words, for the problem (1.15) we see that the dead-core $[a, 1-a]$ appears if ϕ satisfies the condition (1.16).

1.3 Previous studies

There is a vast number of articles devoted to the models (1.15) for various pellet geometries, cf. [2], [4]). Similar models have been studied in [3], [1], and [16]. Particularly, [1], [16] discussed the model extended to the case of external mass transfer

$$\begin{aligned} &\frac{1}{x^s}\frac{d}{dx}\left(x^s \frac{dc}{dx}\right) - \phi^2 r(c) = 0, \quad \text{in } (0,1) \\ &\frac{dc}{dx}(1) - Bi_m(1 - c(1)) = 0, \\ &\frac{dc}{dx}(0) = 0, \end{aligned} \tag{1.17}$$

where $c(x)$ is concentration, Bi_m is a positive constant called Biot number, and $r(c) = [c]_+^p$ is reaction rate, the same as in (1.15). The parameter s stands for for the

pellet geometry, i.e., $s = 0, 1, 2$ corresponds to the planar, cylindrical and spherical geometries respectively.

Andreev in [1] has determined the critical Thiele modulus

$$\phi^* = \sqrt{\frac{2}{1-p}\left(\frac{1+p}{1-p} + s\right)}\left\{1 + \frac{2}{Bi_m(1-p)}\right\}^{(p-1)/2}. \tag{1.18}$$

For $\phi > \phi^*$ the solution to (1.17) has a dead-core, for $\phi < \phi^*$ the solution to (1.17) has no dead-core. This case is also discussed in [16]. Authors considered dead-core and non-dead-core solutions for the above problem, and they also specified the dead-core interval $[0, x_{dz}]$. The time-dependent version of (1.15) was considered in [13], where the author proved that time-dependent solution converges to the stationary one. The similar case but with external mass transfer was studied in [14].

In this thesis two types of model problems with dead-core phenomena are considered: one-dimensional reaction-diffusion problem with Robin boundary conditions and two-dimensional problems with dead-core inside the domain or at the boundary of the domain. Particularly, in Chapter 2, this manuscript improves results of [14] for the one-dimensional problem. In Chapter 3, two-dimensional problems with Dirichlet boundary conditions and power-law reaction kinetics in the reactor domain are considered first. Then, the essence of this thesis will be presented, namely the model for the dead-core at the catalytically active reactor walls. Both problems are solved numerically by spatial discretization via Finite Element method and time-stepping approach through Crank-Nicolson method. Chapter 4 provides error analysis of the finite element solution for the steady-state problems of two-dimensional models from Chapter 3. In Chapter 5, numerical results of simulations for two-dimensional models are discussed and compared with theoretical predictions from other works.

Chapter 2

One-dimensional model for catalytic reactor

2.1 Mathematical model

In the following, the one-dimensional model with Robin boundary conditions is considered. The preliminary results for this model have been presented in the Capstone Project [14]. As mentioned in Introduction, the proofs [14] will be corrected. Let us consider the following model

$$\begin{aligned} u_t - u_{xx} + \phi^2 u_+^p = 0, \quad &\text{in} \quad (0,1)\times(0,\infty)\,, \\ u_x(1,t) + Bi_m(u(1,t)-1) = 0, \quad &\text{for} \quad t\in(0,\infty)\,, \\ u_x(0,t) = 0, \quad &\text{for} \quad t\in(0,\infty), \\ u(x,0) = 1, \quad &\text{in} \quad (0,1)\,. \end{aligned} \tag{2.1}$$

Considering the parabolic problem is essential for numerical investigation in further chapters. Thus, similar to [13], the large time behavior of the solution to the time-dependent problem is analyzed and compared with the solution of steady-state prob-

lem

$$\begin{aligned} \frac{1}{x^s}\frac{d}{dx}(x^s\frac{du}{dx}) - \lambda u_+^p = 0\,, \quad \text{in} \quad (0,1) \\ \frac{du}{dx}(0) = 0\,, \\ \frac{du}{dx}(1) + Bi_m(u(1)-1) = 0\,, \end{aligned} \tag{2.2}$$

where $s = 0, 1, 2$ is the shape factor corresponding to the planar, infinite length cylinder and spherical geometries, respectively. For instance, if $s = 0$, which corresponds to the planar pellet geometry, then (2.2) becomes

$$\begin{aligned} -u_{xx} + \lambda u_+^p = 0\,, \quad \text{in} \quad (0,1) \\ u_x(0) = 0\,, \\ u_x(1) + Bi_m(u(1)-1) = 0\,. \end{aligned} \tag{2.3}$$

2.2 Existence and uniqueness of solution

The existence of a solution for (2.1) can be established using results from [8, p.201]. For the stationary case (2.2) the existence of solution is shown in [8, p. 74]. To show that this solution is also unique, the following lemma will be proved.

Lemma 1 *Let u, v be solutions to (2.2), then $u = v$ for $x \in (0,1)$, $t \in [0,\infty)$.*

Proof. Since u, v are solutions to (2.2), the following holds true

$$\begin{aligned} \frac{1}{x^s}\frac{d}{dx}\Big(x^s\frac{du}{dx}\Big) - \lambda u_+^p = 0\,, \\ \frac{1}{x^s}\frac{d}{dx}\Big(x^s\frac{dv}{dx}\Big) - \lambda v_+^p = 0\,. \end{aligned}$$

Then, we have that

$$-\frac{1}{x^s}\frac{d}{dx}\Big(x^s\frac{dv}{dx}\Big) + \frac{1}{x^s}\frac{d}{dx}\Big(x^s\frac{du}{dx}\Big) + \lambda(v_+^p - u_+^p) = 0\,.$$

Simplifying the above expressions, we obtain

$$-\frac{1}{x^s}\big(x^s(v-u)_x\big)_x + \lambda(v_+^p - u_+^p) = 0\,.$$

Multiplying the above equation by $x^s(v-u)$ and integrating with respect to x over $(0,1)$ leads to

$$-\int_0^1 \big(x^s(v-u)_x\big)_x(v-u)dx + \int_0^1 \lambda(v_+^p - u_+^p)(v-u)dx = 0\,.$$

Integrating by parts the first integral, the following holds true

$$\int_0^1 x^s\Big[(v-u)_x\Big]^2 dx + \int_0^1 \lambda(v_+^p - u_+^p)(v-u)dx = x^s(v-u)_x(v-u)\Big|_0^1,$$

which, using the boundary conditions leads to

$$\int_0^1 x^s\Big[(v-u)_x\Big]^2 dx + \int_0^1 \lambda(v_+^p - u_+^p)(v-u)dx = -Bi_m\big(v(1)-u(1)\big)^2\,. \tag{2.4}$$

Now, LHS ≥ 0 and RHS ≤ 0. Since LHS = RHS, then both sides of the equation must be zero. Thus,

$$v(1) = u(1) \tag{2.5}$$

Then, from (2.4) we also have $v-u = C$. However, $C = 0$ due to (2.5). Hence, $u = v$. □

In the next section we define upper and lower solutions for the time-dependent problem.

2.3 Definition of upper and lower solutions

We define upper and lower solutions similar to [13].

Definition 2 *A function $\bar{u}$ is called an upper solution of the problem* (2.1) *if it sat-*

isfies the following

$$\begin{aligned} \bar{u}_t - \bar{u}_{xx} + \phi^2 \bar{u}_+^p \geq 0, &\quad \textit{in } \mathcal{Q}\,, \\ \bar{u}_x(1,t) + Bi_m(\bar{u}(1,t) - 1) \geq 0, &\quad \textit{for } t \in (0,\infty)\,, \\ \bar{u}_x(0,t) \geq 0, &\quad \textit{for } t \in (0,\infty)\,, \\ \bar{u}(x,0) \geq 1, &\quad \textit{in } (0,1)\,. \end{aligned} \tag{2.6}$$

Similarly, $\underline{u}$ is called a lower solution if the above inequality signs are reversed.

We can provide more information on relation between $u, \bar{u}, \underline{u}$ by proving lemma similar to Lemma 5 in [6]:

Lemma 3 *Let $u(x,t)$ be a solution to the problem* (2.1) *, and $\bar{u}(x,t), \underline{u}(x,t)$ be upper and lower solutions of problem* (2.1)*, respectively. Then, we have $\underline{u}(x,t) \leq u(x,t) \leq \bar{u}(x,t)$.*

Proof. Define $y(x,t) = \bar{u} - \underline{u}$. Then, by mean value theorem, $y(x,t)$ satisfies the following

$$\begin{aligned} y_t - y_{xx} \geq -\phi^2 \frac{\partial f}{\partial u}(\eta) y, &\quad \text{in } \mathcal{Q}, \\ y_x(1,t) + Bi_m y(1,t) \geq 0, &\quad \text{for } t \in (0,\infty), \\ y_x(0,t) \geq 0, &\quad \text{for } t \in (0,\infty), \\ y(x,0) \geq 0, &\quad \text{in } (0,1), \end{aligned}$$

where η is intermediate value between $\bar{u}$ and $\underline{u}$, and $f(\eta) = \eta_+^p$. Now, we can use Lemma 2.1 from [12, p. 54] to obtain $y \geq 0$. Thus, $\bar{u} \geq \underline{u}$. Since u can be considered as an upper or lower solution, we have the following $\underline{u}(x,t) \leq u(x,t) \leq \bar{u}(x,t)$. □

2.4 Boundedness and monotonicity of solution

The weak solution to the non-stationary problem is defined as follows.

Definition 4 *The function $u : [0,1] \to \mathbb{R}$, $u \in H^1(0,1)$, is called a weak solution to* (2.1) *if it satisfies*

$$\int_0^1 u_x(x,t)\psi_x(x) + \phi^2 u_+^p(x,t)\psi(x)dx = Bi_m\psi(1)(1-u(1,t)).$$

for all $\psi \in H^1(0,1)$.

Lemma 5 *Let $u \in H^1(0,1)$ be the weak solution to the boundary value problem* (2.2). *Then, it holds true $0 \le u(x) \le 1$ for all $0 \le x \le 1$.*

Proof. We will prove for upper and lower bounds separately. To find the upper bound, we multiply the differential equation (2.2) by $x^s(u(x)-1)_+$, and integrate by parts over the interval $(0,1)$ to obtain

$$-\int_0^1 z^s \left[\frac{\partial (u-1)_+}{\partial z}(z)\right]^2 dz = Bi_m(u(1)-1)_+^2 + \int_0^1 \lambda z^s (u(z)-1)_+ u_+^p(z)dz\,.$$

Consequently, $(u(x)-1)_+ = 0$ due to the fact that the right hand side of the last equation is non-negative but the left hand side is non-positive. Thus, $u(x) \le 1$ for $0 \le x \le 1$,. Let $u\_ = \min\{u, 0\}$ denote the negative part of u. Multiplying the differential equation (2.2) by $x^s u\_(x)$ and integrating by parts yields

$$-\int_0^1 z^s \left[\frac{\partial u_-}{\partial z}(z)\right]^2 dz + Bi_m u_-(1) = Bi_m u_-(1)u(1) + \int_0^1 \lambda z^s u_-(z) u_+^p(z)dz.$$

Here, notice that the left-hand side is non-positive, while the right-hand side is non-negative. It implies that $u_-(x) = 0$. Thus, $u(x) \ge 0$ for all $0 \le x \le 1$. $\square$

Next, let us show the monotonicity of solutions to problem (2.2) with respect to the reaction rate constant $\lambda > 0$.

Lemma 6 *Let $\lambda_1 \ge \lambda_2 \ge 0$, $p \in (0,1)$, and u_1 and u_2 be solutions to the boundary value problem* (2.2) *with reaction rate constants λ_1 and λ_2, respectively. Then, $u_1(x) \le u_2(x)$ for all $0 \le x \le 1$ with $Bi_m = Bi_{m_1} = Bi_{m_2}$.*

Proof. Since u_1 and u_2 solve the boundary value problem (2.2) with reaction rate constants λ_1 and λ_2, respectively, we have

$$\frac{1}{x^s}\frac{\partial}{\partial x}\left(x^s\frac{\partial u_1}{\partial x}\right) - \frac{1}{x^s}\frac{\partial}{\partial x}\left(x^s\frac{\partial u_2}{\partial x}\right) = \lambda_1[u_1]_+^p - \lambda_2[u_2]_+^p$$

in $(0,1)$. Multiplying the above equation by $x^s(u_1-u_2)_+$ and integrating by parts with further simplifications yields

$$\begin{aligned}
&\int_0^1 z^s\left[\frac{\partial([u_1-u_2]_+)}{\partial z}(z)\right]^2 dz \\
&= Bi_m(u_2(1)-u_1(1))(u_1(1)-u_2(1))_+ \\
&\quad - \int_0^1 z^s(\lambda_1[u_1]_+^p(z) - \lambda_2[u_2]_+^p(z))(u_1-u_2)_+(z))dz \\
&= -Bi_m(u_1(1)-u_2(1))^2 - \lambda_1\int_0^1 z^s([u_1]_+^p(z) - [u_2]_+^p(z))(u_1-u_2)_+(z)dz \\
&\quad - (\lambda_1-\lambda_2)\int_0^1 z^s[u_2]_+^p(z)(u_1-u_2)_+(z)dz.
\end{aligned}$$

Then, assuming $k_1 \geq k_2 \geq 0$ one can observe that

$$\begin{aligned}
\int_0^1 z^s\left[\frac{\partial([u_1-u_2]_+)}{\partial z}(z)\right]^2 dz \leq &- Bi_m(u_1(1)-u_2(1))^2 \\
&- \lambda_1\int_0^1 z^s([u_1]_+^p(z) - [u_2]_+^p(z))(u_1-u_2)_+(z)dz.
\end{aligned}$$

Notice that the left hand side is non-negative, while the right hand side is non-positive. Therefore, $[u_1-u_2]_+(x) = 0$ for $x \in (0,1)$. This means that $u_1(x) \leq u_2(x)$ for $x \in (0,1)$. $\square$

Lemma 7 *Let $\lambda_1 \geq \lambda_2 \geq 0$, $p \in (0,1)$, and u_1 and u_2 be solutions to the boundary value problem (1) with reaction rate constants λ_1 and λ_2, respectively. Then, $u_1(x) \leq u_2(x)$ for all $0 \leq x \leq 1$ with $Bi_{m_1} < Bi_{m_2}$.*

Proof. As in the previous lemma, since u_1 and u_2 solve the boundary value problem (1) with reaction rate constants λ_1 and λ_2, respectively, we have

$$\frac{1}{x^s}\frac{\partial}{\partial x}\left(x^s\frac{\partial u_1}{\partial x}\right) - \frac{1}{x^s}\frac{\partial}{\partial x}\left(x^s\frac{\partial u_2}{\partial x}\right) = \lambda_1[u_1]_+^p - \lambda_2[u_2]_+^p$$

for $x \in (0,1)$. Multiplying the above equation by $x^s(u_1-u_2)_+$ and integrating by parts yields

$$\begin{aligned}
&\int_0^1 z^s\left[\frac{\partial([u_1-u_2]_+)}{\partial z}(z)\right]^2 dz \\
&= \Big[Bi_{m_1}(1-u_1(1)) - Bi_{m_2}(1-u_2(1))\Big]\cdot\Big[u_1(1)-u_2(1)\Big]_+ \\
&\quad - \int_0^1 z^s(\lambda_1[u_1]_+^p(z) - \lambda_2[u_2]_+^p(z))(u_1-u_2)_+(z))dz \\
&= \Big[Bi_{m_1}(u_2(1)-u_1(1)) + (Bi_{m_1}-Bi_{m_2})(1-u_2(1))\Big]\cdot\Big[u_1(1)-u_2(1)\Big]_+ \\
&\quad - \lambda_1\int_0^1 z^s([u_1]_+^p(z) - [u_2]_+^p(z))(u_1-u_2)_+(z)dz \\
&\quad - (\lambda_1-\lambda_2)\int_0^1 z^s[u_2]_+^p(z)(u_1-u_2)_+(z)dz \\
&= -Bi_{m_1}\big[u_1(1)-u_2(1)\big]_+^2 - (Bi_{m_2}-Bi_{m_1})(1-u_2(1))\big[u_1(1)-u_2(1)\big]_+ \\
&\quad - \lambda_1\int_0^1 z^s([u_1]_+^p(z) - [u_2]_+^p(z))(u_1-u_2)_+(z)dz \\
&\quad - (\lambda_1-\lambda_2)\int_0^1 z^s[u_2]_+^p(z)(u_1-u_2)_+(z)dz.
\end{aligned}$$

Since $\lambda_1 \geq \lambda_2 \geq 0$, we have the following inequality

$$\begin{aligned}
0 &\leq \int_0^1 z^s\left[\frac{\partial([u_1-u_2]_+)}{\partial z}(z)\right]^2 dz \\
&\leq -Bi_{m_1}\big[u_1(1)-u_2(1)\big]_+^2 \\
&\quad - (Bi_{m_2}-Bi_{m_1})(1-u_2(1))\big[u_1(1)-u_2(1)\big]_+ \\
&\quad - \lambda_1\int_0^1 z^s\big[(u_1)_+^p(z) - (u_2)_+^p(z)\big]\big[u_1-u_2\big]_+(z).
\end{aligned}$$

From $Bi_{m_1} < Bi_{m_2}$ it follows

$$\begin{aligned} 0 &\leq \int_0^1 z^s \left[\frac{\partial([u_1-u_2]_+)}{\partial z}(z)\right]^2 dz \\ &\leq -\lambda_1 \int_0^1 z^s([u_1]_+^p(z) - [u_2]_+^p(z))(u_1-u_2)_+(z)dz \leq 0. \end{aligned}$$

Assuming $\lambda_1 \geq \lambda_2 \geq 0$ and $(u_+^p - v_+^p)(u-v)_+ \geq 0$ for $x \in (0,1)$ we obtain $[u_1-u_2]_+ = 0$ for $x \in (0,1)$. This means that $u_1 \leq u_2$ in $(0,1)$. $\square$

Another important property of the weak solution is the Lipschitz continuity with respect to the parameter λ. To this end, we will employ the $C^0[0,1]$ norm, which is defined as

$$||v||_{C^0[a,b]} = \max_{a \leq x \leq b} |v(x)|\,.$$

2.5 Lipschitz continuity with respect to the reaction rate constant

Now, we switch to the model (2.3) for the planar pellet geometry. In [14] author proved the following Lipschitz continuity of u with respect to the parameter λ

$$||u(\cdot;\lambda_1) - u(\cdot;\lambda_2)||_{C^0[0,1]} \leq K|\lambda_1 - \lambda_2|,$$

where K is a positive constant. However, the proof will be improved and the exact value of K will be specified. To this end, we prove the following lemma.

Lemma 8 *Let $v(x) = u(x;\lambda_1) - u(x;\lambda_2)$ with $0 \leq \lambda_1 \leq \lambda_2$ and assume that $z(x)$ is a solution of the boundary value problem*

$$\begin{aligned} z''(x) &= \lambda_1 - \lambda_2 \qquad \text{in } (0,1) \\ z'(1) &= -Bi_m z(1), \\ z'(0) &= 0. \end{aligned} \tag{2.7}$$

Then, $v(x) \le z(x)$ *for* $x \in (0,1)$.

Proof. Using the definition of $v(x)$, we find that $v(x)$ is a solution to the following boundary value problem

$$\begin{aligned} v''(x) &= \lambda_1 u^p(x;\lambda_1) - \lambda_2 u^p(x;\lambda_2) \quad \text{in } (0,1) \\ v'(1) &= -Bi_m v(1), \\ v'(0) &= 0. \end{aligned}$$

Now, let us consider the boundary value problem for $v(x) - z(x)$

$$\begin{aligned} (v-z)''(x) &= \lambda_1 u^p(x;\lambda_1) - \lambda_2 u^p(x;\lambda_2) - (\lambda_1 - \lambda_2) \quad \text{in } (0,1) \\ (v-z)'(1) &= -Bi_m(v(1) - z(1)), \\ (v-z)'(0) &= 0. \end{aligned} \tag{2.8}$$

Multiplying (2.8) by $v(x) - z(x)$ and integrating by parts we obtain

$$\begin{aligned} &-\int_0^1 \big[(v-z)'(x)\big]^2 dx - Bi_m\big[v(1)-z(1)\big]^2 \\ &\quad = \int_0^1 \big(\lambda_1 u_1^p - \lambda_2 u_2^p\big)\big(v(x)-z(x)\big)dx - \int_0^1 \big(\lambda_1 - \lambda_2\big)\big(v(x)-z(x)\big)dx \\ &\quad = \int_0^1 \big(\lambda_1 - \lambda_2\big)\big(u_1^p - 1\big)\big(v(x)-z(x)\big)dx + \int_0^1 \lambda_2\big(u_1^p - u_2^p\big)\big(v(x)-z(x)\big)dx \\ &\quad = \int_0^1 \Big[(\lambda_2 - \lambda_1)(1-u_1^p) + \lambda_2(u_1^p - u_2^p)\Big]\Big[v(x)-z(x)\Big]dx, \end{aligned}$$

where $u_1 = u(x;\lambda_1), u_2 = u(x;\lambda_2)$. Since $0 \le \lambda_1 \le \lambda_2$, we can use monotonicity principle $u(x;\lambda_1) \ge u(x;\lambda_2)$. We see that the left hand side is non-positive. Hence, the right hand side is also non-positive. Thus, we have $v(x) - z(x) \le 0$, and so $v(x) \le z(x)$ for $x \in (0,1)$. $\square$

Now, we can show the Lipschitz continuity with respect to the parameter λ.

Lemma 9 *(Lipschitz continuity) There exists a constant* $K = \frac{2+Bi_m}{2Bi_m}$*, such that*

$$\| u(\cdot;\lambda_1) - u(\cdot;\lambda_2) \|_{C^0[0,1]} \leq K|\lambda_1 - \lambda_2|. \tag{2.9}$$

Proof. We use the definition of $v(x), z(x)$ from previous lemma. Solving (2.7) for $z(x)$ results in

$$z(x) = \frac{\lambda_1 - \lambda_2}{2}(x^2 - 1) - \frac{\lambda_1 - \lambda_2}{Bi_m}.$$

Since $v(x) \leq z(x)$, we have the following

$$v(x) \leq \max_{0\leq x\leq 1} z(x) = z(0) = \frac{2 + Bi_m}{2Bi_m}(\lambda_2 - \lambda_1).$$

Thus, $v(x)$ is bounded

$$0 \leq v(x) \leq \frac{2 + Bi_m}{2Bi_m}(\lambda_2 - \lambda_1)$$

which leads to (2.9) with $K = \frac{2+Bi_m}{2Bi_m}$. $\square$

2.6 Derivative of u with respect to λ

In the following, we correct the proof of the upper and lower bounds for derivative of u with respect to λ stated [14]. The derivative of u with respect to λ is defined as follows

$$\lim_{\varepsilon\to 0} \frac{u(\cdot;\lambda+\varepsilon) - u(\cdot;\lambda)}{\varepsilon} = \frac{\partial}{\partial\lambda} u(\cdot;\lambda) \in L^q[(0,1)]. \tag{2.10}$$

In [14], the upper bound to the derivative of u with respect to λ

$$\frac{\partial u(\cdot;\lambda)}{\partial\lambda} \leq 0$$

is also deduced. Furthermore, it also stated in [14] that for v_ε defined below

$$v_\varepsilon(x) = \frac{u(\cdot;\lambda+\varepsilon) - u(\cdot;\lambda)}{\varepsilon}, \tag{2.11}$$

one can show that the following holds true

$$v_\varepsilon''(x) - \lambda p u^{p-1}(x;\lambda) v_\varepsilon(x) < u^p(x;\lambda+\varepsilon) < u^p(x;\lambda), \tag{2.12}$$

in $P_\lambda = (0,1)\backslash N_\lambda$, where $N_\lambda = \{x \in (0,1) :\ u(x) = 0\}$.

Lemma 10 *Let $0 < p < 1$, and for $\varepsilon > 0$ let v_ε be defined as in (2.11) with $\frac{\partial v_\varepsilon}{\partial x}(1) = -Bi_m v_\varepsilon(1)$. Then,*

$$v_\varepsilon(x) \geq -\frac{1}{\lambda(1-p)}\left(\frac{u^p(x;\lambda)}{p} - u(x;\lambda)\right).$$

Proof. Based on the work by Ricci [13], we define

$$z(x) = v_\varepsilon(x) + \frac{1}{\lambda(1-p)}\left(\frac{u^p(x:\lambda)}{p} - u(x;\lambda)\right).$$

Since $u(x;\lambda) = 0$ for $x \in N_\lambda$, then $z(x) = 0$ for $x \in N_\lambda$ as well. Furthermore, we have

$$\begin{aligned}
z'' - \lambda p u^{p-1} z &= v_\varepsilon'' + \frac{1}{\lambda(1-p)}\Big[(p-1)u^{p-2}(u')^2 + u^{p-1}u'' - u''\Big] \\
&\quad - \lambda p u^{p-1} v_\varepsilon - \frac{1}{\lambda(1-p)}\Big[\lambda u^{p-1}u^p - \lambda p u^{p-1} u\Big] \\
&= v_\varepsilon'' - \lambda p u^{p-1} v_\varepsilon + \frac{1}{\lambda(1-p)}\Big[(p-1)u^{p-2}(u')^2 - u'' + \lambda u^p u^{p-1} - \lambda u^p\Big] \\
&< u + \frac{1}{\lambda(1-p)}\Big[(p-1)u^{p-2}(u')^2 + (p-1)u''\Big] \\
&< u - \frac{1}{\lambda}\Big[u^{p-2}(u')^2 + \lambda u^p\Big] = -\frac{1}{\lambda}u^{p-2} \leq 0,
\end{aligned}$$

where $u(\cdot;\lambda)$ is indicated by u. Now, we only need to discuss the boundary condition at $x = 1$. We have

$$\begin{aligned}
z'(x) &= v_\varepsilon'(x) + \frac{1}{\lambda(1-p)}\Big[u^{p-1}u' - u'\Big], \\
Bi_m z(1) &= Bi_m\left[v_\varepsilon(1) + \frac{1}{\lambda(1-p)}\Big(\frac{u^p(1;\lambda)}{p} - u(1;\lambda)\Big)\right]
\end{aligned} \tag{2.13}$$

from which we infer that

$$
\begin{aligned}
z'(1) &= v'_\varepsilon(1) + \frac{1}{\lambda(1-p)}\Big[u^{p-1}(1;\lambda)u'(1;\lambda) - u'(1;\lambda)\Big] \\
&= -Bi_m v_\varepsilon(1) + \frac{1}{\lambda(1-p)}\Big[u'(1;\lambda)(u^{p-1}(1;\lambda)-1)\Big] \\
&= -Bi_m v_\varepsilon(1) + \frac{1}{\lambda(1-p)}\Big[Bi_m(1-u(1;\lambda))(u^{p-1}(1;\lambda)-1)\Big] \\
&= -Bi_m v_\varepsilon(1) + \frac{Bi_m}{\lambda(1-p)}\Big[(1-u(1;\lambda))(u^{p-1}(1;\lambda)-1)\Big] \\
&= -Bi_m v_\varepsilon(1) + \frac{Bi_m}{\lambda(1-p)}\Big[u^{p-1}(1;\lambda) - u^p(1;\lambda) + u(1;\lambda) - 1\Big].
\end{aligned}
$$

Now, combining the latter with (2.13) we obtain

$$
\begin{aligned}
z'(1) + Bi_m z(1) &= \frac{Bi_m}{\lambda(1-p)}\left[u^{p-1}(1;\lambda) - u^p(1;\lambda) - 1 + \frac{u^p(1;\lambda)}{p}\right] \\
&= \frac{Bi_m}{\lambda(1-p)}\left[u^{p-1}(1;\lambda) - u^p(1;\lambda)\Big(1-\frac{1}{p}\Big) - 1\right] \\
&= \frac{Bi_m}{\lambda(1-p)}\left[-\frac{p-1}{p}u^p(1;\lambda) + u^p(1;\lambda) - 1\right] \\
&= \frac{Bi_m}{\lambda(1-p)}\left[\frac{1-p}{p}u^p(1;\lambda) + u^{p-1}(1;\lambda) - 1\right].
\end{aligned}
$$

Hence, $z(x)$ solves

$$
z'' - \lambda p u^{p-1} z < 0, \quad \text{in} \quad P_\lambda\,, \tag{2.14}
$$

$$
z = 0, \quad \text{in} \quad N_\lambda\,, \tag{2.15}
$$

$$
z'(1) + Bi_m z(1) = \gamma(1)\,, \tag{2.16}
$$

where for $x \in (0,1]$ is defined as

$$
\gamma(x) = B_{i_m}\frac{1}{\lambda(1-p)}\left[\frac{1-p}{p}u^p(x;\lambda) + u^{p-1}(x;\lambda) - 1\right].
$$

Note that $\gamma(x) \geq 0$, since

$$\begin{aligned}\gamma(x) &= \frac{Bi_m}{\lambda p(1-p)}\Big[(1-p)u^p + pu^{p-1} - p\Big] \\ &= \frac{Bi_m}{\lambda p(1-p)}\Big[(1-p)u^p + \frac{pu^p}{u} - p\Big] \\ &= \frac{Bi_m}{\lambda p(1-p)u}\Big[(1-p)u^{p+1} + pu^p - pu\Big] \\ &= \frac{Bi_m}{\lambda p(1-p)u}\Big[(1-p)u^{p+1} + p(u^p - u)\Big] \geq 0,\end{aligned}$$

where $u = u(x;\lambda)$. We also used facts that $0 \leq u(x;\lambda) \leq 1$, and $u^p(x;\lambda) \geq u(x;\lambda)$. Now, we have to show that $z(x) \geq 0$. We already know that $z(x) = 0$ for $x \in N_\lambda$. Thus, we should discuss it for $x \in P_\lambda$. Suppose that $z(x)$ has negative local minimum, then we contradict (2.14), thus if there is local minimum for $x \in P_\lambda$, then it has to be positive. However, we could obtain negative absolute minimum at $x = 1$, but this contradicts with (2.16). Thus, $z(x) \geq 0$, which means that we have the lower bound for $v_\varepsilon(x)$ as follows

$$v_\varepsilon(x) \geq -\frac{1}{\lambda(1-p)}\Big(\frac{u^p(x;\lambda)}{p} - u(x;\lambda)\Big). \tag{2.17}$$

□

Taking the limit $\varepsilon \to 0^+$, the L^∞ estimate is preserved and we get

$$0 \geq \frac{\partial u}{\partial \lambda}(x;\lambda) \geq -\frac{1}{\lambda(1-p)}\Big(\frac{u^p(x;\lambda)}{p} - u(x;\lambda)\Big). \tag{2.18}$$

2.7 Construction of upper and lower solutions

In [14] the upper and lower solutions were constructed for the case $\lambda = 1$. In the following, this result will be improved for the general ϕ^2 which will allow us to complete the proof of convergence of the time-dependent solution to the stationary one. As in

the original work, we start with a positive function $\mu \in C^1([0,+\infty))$. Let

$$\tilde{u}(x,t) = u(x;\mu(t))\,,$$

where $u(x;\mu(t))$ is the unique solution of elliptic problem

$$\begin{aligned} -u_{xx} + \lambda u_+^p &= 0, \\ u_x(1) + Bi_m(u(1)-1) &= 0, \\ u_x(0) &= 0, \end{aligned} \tag{2.19}$$

with $\lambda = \mu(t)$. Let us define the linear operator $\mathcal{L}$ as follows

$$\mathcal{L}(\tilde{u}) = \tilde{u}_t - \tilde{u}_{xx} + \phi^2 \tilde{u}_+^p = \frac{\partial u}{\partial \lambda}(x;\mu(t))\mu'(t) - \left[\mu(t) - \phi^2\right] u_+^p(x;\mu(t))\,.$$

Here, note that $\tilde{u}_{xx} = \mu(t)u_+^p = \mu(t)u_+^p(x;\mu(t))$ since $\tilde{u}$ is the solution of elliptic problem. Suppose now that $\mu'(t) > 0$. Then,

$$\frac{\partial u}{\partial \lambda}(x;\lambda) \geq -\frac{u^p(x;\lambda)}{\lambda(1-p)p}\,,$$

and we get

$$\mathcal{L}(\tilde{u}) \geq \left[-\frac{\mu'(t)}{\mu(t)(1-p)p} + \phi^2 - \mu(t)\right] u_+^p(x;\mu(t))\,. \tag{2.20}$$

Conversely, if $\mu'(t) < 0$, the sign in Eq. (2.20) the sign is reversed and it becomes

$$\mathcal{L}(\tilde{u}) \leq \left[-\frac{\mu'(t)}{\mu(t)(1-p)p} + \phi^2 - \mu(t)\right] u_+^p(x;\mu(t))\,. \tag{2.21}$$

Let $\mu(t)$ be such that

$$\mu'(t) = \mu(t)p(1-p)(\phi^2 - \mu(t)). \tag{2.22}$$

Solving the above differential equation for $\mu(t)$ by separation of variables yields

$$\begin{aligned}
\int_{\mu_0}^{\mu} \frac{d\mu}{\mu(\phi^2-\mu)} &= \int_0^T p(1-p)dt \\
\frac{1}{\phi^2}\big[\log(\mu)-\log(1-\mu)\big]\Big|_{\mu_0}^{\mu} &= p(1-p)t \\
\frac{\frac{\phi^2}{\mu_0}-1}{\frac{\phi^2}{\mu}-1} &= \exp(\phi^2 p(1-p)t) \\
\mu(t) &= \phi^2[1+(\phi^2/\mu_0-1)\exp(-\phi^2 p(1-p)t)]^{-1},
\end{aligned}$$

where $\mu_0 = \mu(0)$. Now, we have two cases: $\mu_0 < \phi^2$, and $\mu_0 > \phi^2$.

Case 1: $\mu_0 < \phi^2$

$$\begin{aligned}
&\frac{\phi^2}{\mu_0} - 1 > 0\,, \\
&1 + \Big(\frac{\phi^2}{\mu_0} - 1\Big)\exp(-\phi^2 p(1-p)t) > 1\,, \\
&\mu < \phi^2\,.
\end{aligned}$$

Thus, from equation (2.22) we see that $\mu'(t) > 0$, therefore $\mathcal{L}(\tilde{u}) \geq 0$ meaning that $\tilde{u}(x,t)$ is an upper solution of the problem (2.1) with initial data

$$u(x;\phi^2) \leq u_0(x) = u(x;\mu_0) \leq 1\,. \tag{2.23}$$

Case 2: $\mu_0 > \phi^2$

Analogously, $\mu > \phi^2$ which means that $\mu'(t) < 0$ from (2.22). Thus, $\mathcal{L}(\tilde{u}) \leq 0$ meaning that $\tilde{u}$ is now a lower solution of the problem (P) with initial data

$$u(x;\phi^2) \geq u_0(x) = u(x;\mu_0) \geq 0\,, \tag{2.24}$$

where $u(x;\phi^2)$ is the stationary solution of our problem because of $\mu_0 = \phi^2$ in Eq. (2.22).

Now, we are able to show the main theorem of this Chapter.

Theorem 11 *Let* $\mu(t) = \phi^2[1 + (\phi^2/\mu_0 - 1)\exp(-\phi^2 p(1-p)t)]^{-1}$. *Then, if* $\mu_0 < \phi^2$ ($\mu_0 > \phi^2$), *the function* $\tilde{u}(x,t) = u(x;\mu)$ *is an upper (a lower) solution of* (2.1), *corresponding to the initial data* $u_0(x) = u(x;\mu_0) \geq u(x;\phi^2)(\leq)$. *Moreover*

$$\begin{aligned} &\| u(x;\phi^2) - \tilde{u}(x;t) \|_{C^0[0,1]} \\ &\leq \phi^2 \left(\frac{2 + Bi_m}{2Bi_m} \right) \frac{|\phi^2/\mu_0 - 1| \exp(-\phi^2 p(1-p)t)}{1 + (\phi^2/\mu_0 - 1)\exp(-\phi^2 p(1-p)t)} . \end{aligned} \tag{2.25}$$

Notice that this estimate resulted from the Lipschitz continuity of $u(\cdot;\lambda)$. We can show that right hand side of (2.25) converges to 0. For $\mu_0 < \phi^2$, we have the following

$$\begin{aligned} &\phi^2 \frac{2 + Bi_m}{2Bi_m} \frac{(\phi^2/\mu_0 - 1)\exp(-\phi^2 p(1-p)t)}{1 + (\phi^2/\mu_0 - 1)\exp(-\phi^2 p(1-p)t)} \\ &= \phi^2 \frac{2 + Bi_m}{2Bi_m} \frac{(\phi^2/\mu_0 - 1)\exp(-\phi^2 p(1-p)t) + 1 - 1}{1 + (\phi^2/\mu_0 - 1)\exp(-\phi^2 p(1-p)t)} \\ &= \phi^2 \frac{2 + Bi_m}{2Bi_m} \left[1 - \frac{1}{1 + (\phi^2/\mu_0 - 1)\exp(-\phi^2 p(1-p)t)} \right]. \end{aligned}$$

For $\mu_0 > \phi^2$, we have the following

$$\begin{aligned} &\phi^2 \frac{2 + Bi_m}{2Bi_m} \frac{(1 - \phi^2/\mu_0)\exp(-\phi^2 p(1-p)t)}{1 + (\phi^2/\mu_0 - 1)\exp(-\phi^2 p(1-p)t)} \\ &= \phi^2 \frac{2 + Bi_m}{2Bi_m} \frac{-(\phi^2/\mu_0 - 1)\exp(-\phi^2 p(1-p)t)}{1 + (\phi^2/\mu_0 - 1)\exp(-\phi^2 p(1-p)t)} \\ &= \phi^2 \frac{2 + Bi_m}{2Bi_m} \frac{-(\phi^2/\mu_0 - 1)\exp(-\phi^2 p(1-p)t) - 1 + 1}{1 + (\phi^2/\mu_0 - 1)\exp(-\phi^2 p(1-p)t)} \\ &= \phi^2 \frac{2 + Bi_m}{2Bi_m} \left[-1 + \frac{1}{1 + (\phi^2/\mu_0 - 1)\exp(-\phi^2 p(1-p)t)} \right]. \end{aligned}$$

Both bounds in the above estimates converge to 0 as $t \to \infty$.

Chapter 3

Two-dimensional models for catalytic reactors

3.1 Model with volume reaction in catalytic reactor

3.1.1 Model problem

In this section the following boundary value problem is investigated

$$\begin{aligned} -\Delta u + \phi^2 [u]_+^p = 0, \quad & \text{in } \Omega = (0,1)^2, \\ u = 1, \quad & \text{on } \partial\Omega, \end{aligned} \tag{3.1}$$

which is Dirichlet boundary value problem for Eq. (1.13). The corresponding non-stationary model can be written as

$$\begin{aligned} u_t - \Delta u + \phi^2 [u]_+^p = 0, \quad & \text{in } \Omega = (0,1)^2, \text{ for } t \in [0,\infty), \\ u = 1, \quad & \text{on } \partial\Omega\,. \end{aligned} \tag{3.2}$$

The non-stationary problem is solved numerically via Finite Element Method (FEM) and Crank-Nicolson scheme. However, before using FEM we should introduce the weak formulation of the non-stationary problem.

3.1.2 Weak formulation

The weak formulation will be introduced similar to definition in [7, p. 296].

Definition 12 *Let $\psi \in H_0^1(\Omega)$ be the test function and $t \mapsto u(t) \in H^1(0,1)$. Multiplying (3.2) by ψ and integrating over Ω results in*

$$\int_\Omega u_t(x,t)\psi(x)dx + \int_\Omega \nabla u(x,t)\nabla\psi(x)dx + \phi^2 \int_\Omega [u]_+^p(x,t)\psi(x)dx = 0, \tag{3.3}$$

which is a weak formulation for (3.2)

However, (3.3) has a unique weak solution, which was proven by [2] in Theorem 2.1. Analytical dead-core solution for the steady-state problem was discussed in [18]. Thus, solving time-dependent problem numerically will show allow us to approach the unique solution of the steady-state problem.

Remark 13 *Notice that in the Definition 12, $\psi \in H_0^1(\Omega)$ means that $\psi = 0$ on $\partial\Omega$, which is the reason for the absence of boundary terms in the weak formulation.*

3.1.3 Numerical scheme

In order to use FEM, we decompose the spatial reactor domain into small triangles as shown in Figure 4-2. The idea of FEM is to approximate the solution on the small triangles. At each node we find approximate values of u. Note that in this thesis P_1 linear elements are used. Now, (3.3) transforms into

$$\int_\Omega u_t(x,t)\psi_i(x)dx + \int_\Omega \nabla u(x,t)\nabla\psi_i(x)dx + \phi^2 \int_\Omega [u]_+^p(x,t)\psi_i(x)dx = 0, \tag{3.4}$$

where i is the index of a node in Figure 4-2. In the above expression ψ_i is value of ψ at i-th node. Then the ansatz is the following:

$$u_h(x,t) := \sum_{j\in N} u_j(t)\psi_j(x), \tag{3.5}$$

where j runs through the nodes of the mesh. N stands for the number of all nodes of the triangular mesh. Then, by substituting the above ansatz into (3.4) the following equation is obtained

$$\int_\Omega \Big(\sum_{j\in N} \dot{u}_j(t)\psi_j \Big)\psi_i dx + \int_\Omega \Big(\sum_{j\in N} u_j(t)\nabla\psi_j \Big)\nabla\psi_i dx + \int_\Omega \phi^2 \Big(\sum_{j\in N} \Big(u_j(t)\psi_j \Big)_+^p \Big)\psi_i dx = 0\,.$$

Since the integration is in spatial variable, it is reasonable to factor out the functions depending on time t as follows

$$\sum_{j\in N} \Big(\int_\Omega \psi_j\psi_i dx \Big)\dot{u}_j(t) + \sum_{j\in N} \Big(\int_\Omega \nabla\psi_j\nabla\psi_i dx \Big)u_j(t) + \int_\Omega \phi^2 \Big(\sum_{j\in N} \Big(u_j(t)\psi_j \Big)_+^p \Big)\psi_i dx = 0. \tag{3.6}$$

In the above expression $u_j(t)$ could not be factored out due to the nonlinearity of power-type. However, the approximation method from [5] can be employed here and tested numerically later. The method in the latter article is called the product approximation (P.A.) and is based on the following approximation

$$f\Big(\sum_k u_k\psi_k \Big) \approx \sum_k f(u_k)\psi_k. \tag{3.7}$$

Using the P.A. (3.6) implies

$$\sum_{j\in N} \Big(\int_\Omega \psi_j\psi_i dx \Big)\dot{u}_j(t) + \sum_{j\in N} \Big(\int_\Omega \nabla\psi_j\nabla\psi_i dx \Big)u_j(t) + \int_\Omega \phi^2 \sum_{j\in N} \Big(u_j(t) \Big)_+^p \psi_j\psi_i dx = 0\,. \tag{3.8}$$

Factoring out the time-dependent functions from integral in spatial variable the above equation becomes

$$\sum_{j\in N}\Big(\int_\Omega \psi_j\psi_i dx\Big)\dot{u}_j(t)+\sum_{j\in N}\Big(\int_\Omega \nabla\psi_j\nabla\psi_i dx\Big)u_j(t) + \phi^2\sum_{j\in N}\Big(\int_\Omega \psi_j\psi_i dx\Big)\Big(u_j(t)\Big)_+^p=0. \tag{3.9}$$

This can be rewritten in the matrix form

$$M\dot{\boldsymbol{u}}+K\boldsymbol{u}+\phi^2 M[\boldsymbol{u}]_+^p=\boldsymbol{0}, \tag{3.10}$$

where M, K are mass and stiffness matrices whose entries m_{ij}, k_{ij} are defined as follows

$$m_{ij}=\int_\Omega \psi_j\psi_i dx, \quad k_{ij}=\int_\Omega \nabla\psi_j\nabla\psi_i dx. \tag{3.11}$$

Now, since the vector $\boldsymbol{u}$ has some entries equals 1 (due to the Dirichlet boundary conditions), we divide the entries of matrices and vectors accordingly, such that we only look for unknown entries of $\boldsymbol{u}$. In the *MATLAB* the nodes on the mesh are counted such that inner nodes come after boundary nodes. Since in our case $u=1$ on all boundaries, vector $\boldsymbol{u}$ can be partitioned in the following way:

$$\begin{bmatrix}\boldsymbol{u}_D\\ \boldsymbol{u}_I\end{bmatrix},$$

where u_D are Dirichlet nodes and u_I are inner nodes. The matrices in *MATLAB* have similar structure, so that the matrix equation (3.10) can be rewritten as follows:

$$\begin{bmatrix}M_{DD} & M_{DI}\\ M_{ID} & M_{II}\end{bmatrix}\begin{bmatrix}\dot{\boldsymbol{u}}_D\\ \dot{\boldsymbol{u}}_I\end{bmatrix}+\begin{bmatrix}K_{DD} & K_{DI}\\ K_{ID} & K_{II}\end{bmatrix}\begin{bmatrix}\boldsymbol{u}_D\\ \boldsymbol{u}_I\end{bmatrix}+\phi^2\begin{bmatrix}M_{DD} & M_{DI}\\ M_{ID} & M_{II}\end{bmatrix}\begin{bmatrix}\boldsymbol{u}_D\\ \boldsymbol{u}_I\end{bmatrix}_+^p=\boldsymbol{0}, \tag{3.12}$$

where $[\cdot]_+^p$ operation is elementwise, and $M_{DD}, M_{ID}, M_{DI}, M_{II}$ are submatrices of matrix M, submatrices of K are defined analogously. Now, since the vector $\boldsymbol{u}_D$ is known, the dimension of matrix equation can be decreased to the number of inner

nodes only, instead of all nodes. Thus, the desired matrix equation reads as follows

$$M_{II}\dot{\boldsymbol{u}}_I + M_{ID}\dot{\boldsymbol{u}}_D + K_{II}\boldsymbol{u}_I + K_{ID}\boldsymbol{u}_D + \phi^2 M_{ID}[\boldsymbol{u}_D]_+^p + \phi^2 M_{II}[\boldsymbol{u}_I]_+^p = \boldsymbol{0},$$

which is simplified further because $\dot{\boldsymbol{u}}_D = \boldsymbol{0}$ and $[\boldsymbol{u}_D]_+^p = \boldsymbol{u}_D$

$$M_{II}\dot{\boldsymbol{u}}_I + K_{II}\boldsymbol{u}_I + K_{ID}\boldsymbol{u}_D + \phi^2 M_{ID}\boldsymbol{u}_D + \phi^2 M_I[\boldsymbol{u}_I]_+^p = 0. \tag{3.13}$$

Now, after spatial discretization the equation still has time variable involved. We consider the time discretization by Crank-Nicolson scheme, which employs the following approximations

$$\dot{u} \approx \frac{u^{n+1} - u^n}{\Delta t}, \quad u \approx \frac{u^{n+1} + u^n}{2}.$$

Substituting the above into (3.13) the nonlinear system which can be solved for u^{n+1} is obtained

$$\boldsymbol{u}^{n+1} = \left(\frac{1}{\Delta t}M_{II} + \frac{1}{2}K_{II}\right)^{-1}\Big(- K_{ID}\boldsymbol{u}_D - \phi^2 M_{ID}\boldsymbol{u}_D - \phi^2 K_{II}\Big(\frac{\boldsymbol{u}^n + \boldsymbol{u}^{n+1}}{2}, 0\Big)_+^p - \frac{1}{2}K_{II}\boldsymbol{u}^n + \frac{1}{\Delta t}M_{II}\boldsymbol{u}^n\Big). \tag{3.14}$$

The above formula represents the time loop. Additionally, in each step we make an extra projection step

$$\boldsymbol{u}^{n+1} = 0.5\max(\boldsymbol{u}^{n+1}, 0) + 0.5\max(\boldsymbol{u}^n, 0)$$

to ensure the positivity of the approximate solution. The method (see 6.1 in Appendix) is implemented in *MATLAB* software using PDE Toolbox.

3.1.4 Finite element error estimates

In this section the error analysis for the finite element solution of (3.1) will be presented. Let us define the weak formulation and finite element solution.

Definition 14 *Let $\psi \in H_0^1(\Omega)$ be a test function. Multiplying* (3.1) *by ψ and inte-*

grating over Ω *results in*

$$\int_\Omega \nabla u(x,t)\cdot\nabla\psi(x)dx + \phi^2\int_\Omega [u]_+^p(x,t)\psi(x)dx = 0, \tag{3.15}$$

which is a weak formulation for (3.1).

Definition 15 *Let* $V_h \subset H^1(0,1)$ *be a finite element space of piecewise linears. We say that* $u_h \in V_h \subset H_1^1(\Omega)$ *is a finite element solution if it satisfies the following*

$$\int_\Omega \nabla u_h(x)\cdot\nabla\psi_h(x)dx + \phi^2\int_\Omega [u_h]_+^p(x)\psi_h(x)dx = 0 \tag{3.16}$$

for all discrete test functions $\psi_h \in V_h$.

To prove existence of a finite element solution u_h authors of [4] used an equivalent minimization problem: minimize for $\psi \in H_1^1(\Omega)$ the following expression:

$$J(\psi) = \int_\Omega \Big(\frac{1}{2}(\nabla\psi)^2 + \phi^2 F(\psi)\Big)dx, \tag{3.17}$$

where $F(\psi)$ is the following step function:

$$F(z) = \int_0^z [s]_+^p ds = \begin{cases} \frac{z^{p+1}}{p+1}, & \text{for } z \geq 0 \\ 0, & \text{for } z \leq 0, \end{cases}$$

and

$$H_g^1(\Omega) \equiv \{\psi \in H^1(\Omega) : \psi = g \text{ on } \partial\Omega\}.$$

According to [4] the uniqueness follows since $[u_h]_+^p$ is monotonically increasing. Moreover, in [2] authors proved that if $u \in H^2(\Omega)$, then the following error estimates for (3.16) hold

$$|u - u_h|_1 \leq \begin{cases} Ch, & \text{for } \frac{1}{2} \leq p < 1, \\ Ch^{2p}, & \text{for } 0 < p \leq \frac{1}{2}. \end{cases} \tag{3.18}$$

3.2 Model for membrane reactor

3.2.1 Model problem

In this section, the reactor is modified such that the catalytic reaction occur only at the membrane which is represented by a part of domain boundary. For simplicity, the reactor will be represented by the unit square $\Omega = (0,1)^2$. The model with mixed

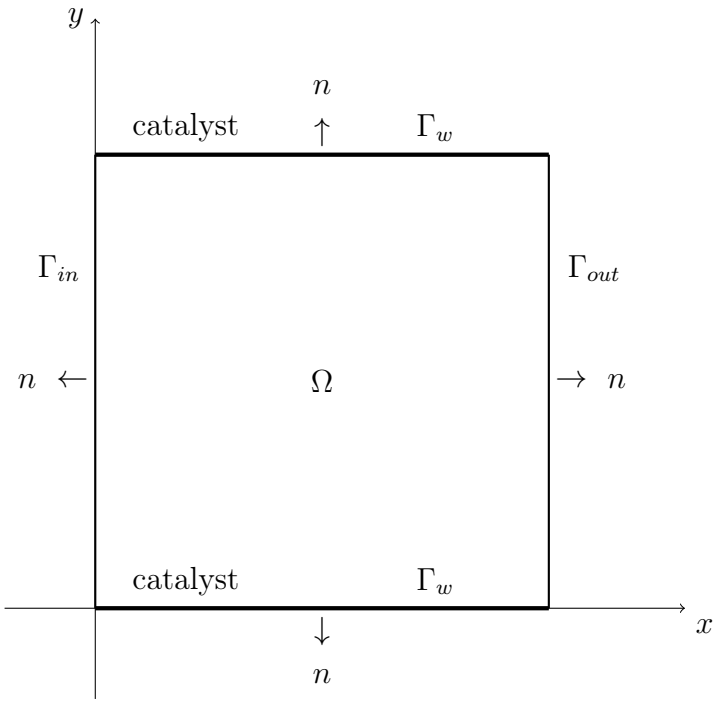

Figure 3-1: Reactor geometry.

boundary conditions reads as follows

$$-\Delta u = 0 \qquad \text{in } \Omega, \tag{3.19}$$

$$\begin{aligned} u &= 1 && \text{on } \Gamma_{in}, \\ -\frac{\partial u}{\partial n} &= \phi^2 [u]_+^p && \text{on } \Gamma_w, \\ -\frac{\partial u}{\partial n} &= 0 && \text{on } \Gamma_{out}, \end{aligned} \tag{3.20}$$

where $\phi^2[u]_+^p$ is the same power law kinetics as in (1.15). Now, let us add time derivative to the equation (3.19) such that the initial/boundary value problem is

given by

$$\begin{aligned} u_t - \Delta u &= 0 && \text{in } \Omega \times [0,\infty), \\ u &= 1 && \text{on } \Gamma_{in}, \\ -\frac{\partial u}{\partial n} &= \phi^2 [u]_+^p && \text{on } \Gamma_w, \\ -\frac{\partial u}{\partial n} &= 0 && \text{on } \Gamma_{out} \end{aligned} \tag{3.21}$$

and $u(x,0) = 1$ for $x \in \Omega$.

3.2.2 Boundedness of a weak solution

Using the weak formulation from previous section on the above time-dependent problem yields the following

Definition 16 *Let $\psi \in H^1_{0,\Gamma_{in}}(\Omega)$ be a test function such that $\psi|_{\Gamma_{in}} = 0$ in the trace sense. Multiplying* (3.21) *by ψ and integrating over Ω results in*

$$\int_\Omega u_t(x,t)\psi(x)dx + \int_\Omega \nabla u(x,t)\nabla\psi(x)dx + \phi^2 \int_{\Gamma_w} [u]_+^p(x,t)\psi(x)dx = 0, \tag{3.22}$$

which is a weak formulation for the problem (3.21)*. Note that* (3.20) *was used to form the last line integral in* (3.22)*.*

In the the steady-state limit (3.22) becomes

$$\int_\Omega \nabla u(x)\nabla\psi(x)dx + \phi^2 \int_{\Gamma_w} [u]_+^p(x)\psi(x)dx = 0, \tag{3.23}$$

which is the weak formulation for (3.19). Notice that the weak solution is $u(x)$ which satisfies (3.23).

Lemma 17 *The weak solution u of* (3.23) *satisfies*

$$0 \le u \le 1. \tag{3.24}$$

Proof. Let us prove the upper bound first. Choose the test function in (3.23) as $[u-1]_+ = \max([u-1], 0)$. Then, the weak formulation reads as

$$\begin{aligned}
&\int_\Omega \nabla u \cdot \nabla [u-1]_+ dx + \phi^2 \int_{\Gamma_w} [u]_+^p [u-1]_+ ds \\
&= \int_\Omega \nabla (u-1) \cdot \nabla [u-1]_+ dx + \phi^2 \int_{\Gamma_w} [u]_+^p [u-1]_+ ds \\
&= \int_\Omega \left| \nabla [u-1]_+ \right|^2 dx + \phi^2 \int_{\Gamma_w} [u]_+^p [u-1]_+ ds = 0 \,.
\end{aligned}$$

The last equation can be rewritten as follows

$$\int_\Omega \left| \nabla [u-1]_+ \right|^2 dx = -\phi^2 \int_{\Gamma_w} [u]_+^p [u-1]_+ ds \,.$$

Since the non-negative and non-positive expressions are equal, it follows that

$$\int_\Omega \left| \nabla [u-1]_+ \right|^2 dx = 0,$$

which means that $[u-1]_+ \equiv C$, where C is a constant. However, $C = 0$ because of Dirichlet boundary condition $u = 1$. Thus, $[u-1]_+ = 0$, which leads to the conclusion that $u \leq 1$. For the lower bound we choose the test function $\psi = [u]_- = \max(-u, 0)$. Then, the weak formulation from (3.23) reads as follows

$$\int_\Omega \nabla u \cdot \nabla [u]_- dx + \phi^2 \int_{\Gamma_w} [u]_+^p [u]_- ds \quad = \int_\Omega \left| \nabla [u]_- \right|^2 dx + \phi^2 \int_{\Gamma_w} [u]_+^p [u]_- ds = 0 \,.$$

The last equation can be rewritten as follows

$$\int_\Omega \left| \nabla [u]_- \right|^2 dx = -\phi^2 \int_{\Gamma_w} [u]_+^p [u]_- ds \,.$$

Since $[u]_+^p [u]_- = 0$, then the right hand side is zero as well. Thus, $\nabla [u]_- = 0$, so $[u]_-$ is constant. Due to the Dirichlet condition, $[u]_- = \max(-1, 0) = 0$. Hence, $u \geq 0$. Thus, (3.24) is proved. $\square$

3.2.3 Numerical scheme

The (3.21) problem is solved numerically by FEM and using the same triangular mesh as in Figure 4-2. As in previous section, piecewise linear elements are used. Hence, the weak formulation is transformed just as in Section 3.1 resulting in the following equation:

$$\int_\Omega \frac{\partial u_h}{\partial t}(x,t)\psi_i(x)dx + \int_\Omega \nabla u_h(x,t)\nabla\psi_i(x)dx + \phi^2 \int_{\Gamma_w} [u_h]_+^p(x,t)\psi_i(x)ds = 0, \quad (3.25)$$

where FEM test functions ψ_i are zero at the boundary part Γ_{in}. Substituting ansatz (3.5) into (3.25) produces the following (with N corresponding to the number of all nodes):

$$\int_\Omega \Big(\sum_{j\in N} \dot{u}_j(t)\psi_j\Big)\psi_i dx + \int_\Omega \Big(\sum_{j\in N} u_j(t)\nabla\psi_j\Big)\nabla\psi_i dx + \phi^2 \int_{\Gamma_w} \Big(\sum_{j\in N} u_j(t)\psi_j\Big)_+^p \psi_j ds = 0,$$

which can be rewritten as

$$\sum_{j\in N}\Big(\int_\Omega \psi_j\psi_i dx\Big)\dot{u}_j(t) + \sum_{j\in N}\Big(\int_\Omega \nabla\psi_j\nabla\psi_i dx\Big)u_j(t) + \phi^2 \int_{\Gamma_w} \Big(\sum_{j\in N} u_j(t)\psi_j\Big)_+^p \psi_i ds = 0.$$

In the above equation the product approximation from [5] is used again to obtain

$$\sum_{j\in N}\Big(\int_\Omega \psi_j\psi_i dx\Big)\dot{u}_j(t) + \sum_{j\in N}\Big(\int_\Omega \nabla\psi_j\nabla\psi_i dx\Big)u_j(t) + \phi^2 \sum_{j\in N}\Big(\int_{\Gamma_w} \psi_j\psi_i ds\Big)\big(u_j(t)\big)_+^p = 0,$$

which can be written in the matrix form as

$$M\dot{\boldsymbol{u}} + K\boldsymbol{u} + \phi^2 Q[\boldsymbol{u}]_+^p = \mathbf{0}, \quad (3.26)$$

where M, K are defined by (3.11) and Q is the matrix with the following entries

$$q_{ij} = \int_{\Gamma_w} \psi_i \psi_j ds. \tag{3.27}$$

In the model from Section 3.1 the boundary condition was of Dirichlet type defined for all parts of $\partial\Omega$. However, in this section we have mixed boundary conditions of Neumann and Dirichlet types. Before solving the matrix equation above, we have to find out the nodes for corresponding boundary conditions. The numbering of nodes in the *MATLAB* is the following: first group of nodes are the vertices of the rectangular domain, then in the corresponding order are left, bottom, top and right edges, following with inner nodes. As an example for the mesh size $h = 0.15$ the numbering of nodes is shown in Figure 4-3. The boundary conditions in the model problem (3.21) suggest that nodes 1, 2 can belong to both Γ_w and Γ_{in}, same as nodes $3, 4$ belong to both Γ_w and Γ_{out}. The problem is that numbering of nodes is not convenient in the way, that Dirichlet boundary conditions have nodes $1, 2, 5, ...$, so nodes $3, 4$ have to be skipped. Since numbering of nodes cannot be changed, the change must be applied to matrices and vectors. The idea is to take out rows and columns $3, 4$ from matrices and vectors and place them after the rows and columns for the corresponding nodes of the Γ_{out} edge of the rectangular domain. In this way, the structure of the solution vector is the following: Γ_{in} nodes, Γ_w nodes, Γ_{out} nodes and inner nodes. Then, the partition of the solution vector is given by

$$[\boldsymbol{u}_d, \boldsymbol{u}_r, \boldsymbol{u}_n, \boldsymbol{u}_i]^T \tag{3.28}$$

where $\boldsymbol{u}_d$ corresponds to the Dirichlet boundary (Γ_{in}), $\boldsymbol{u}_r$ to the reaction on the boundary (Γ_w), $\boldsymbol{u}_n$ stands for the zero Neumann boundary (Γ_{out}) and $\boldsymbol{u}_i$ is for the inner nodes of the domain. Since the unknowns are $\boldsymbol{u}_r, \boldsymbol{u}_n, \boldsymbol{u}_i$, we can group them into the $\boldsymbol{u}_o$, such that the structure of the solution vector is

$$[\boldsymbol{u}_d, \boldsymbol{u}_o]^T. \tag{3.29}$$

The rows and columns of the matrices have to be modified in the same way. The matrices are partitioned into submatrices in the same way, so (3.26) is given by

$$\begin{bmatrix} M_{dd} & M_{do} \\ M_{od} & M_{oo} \end{bmatrix} \begin{bmatrix} \dot{\boldsymbol{u}}_d \\ \dot{\boldsymbol{u}}_o \end{bmatrix} + \begin{bmatrix} K_{dd} & K_{do} \\ K_{od} & K_{oo} \end{bmatrix} \begin{bmatrix} \boldsymbol{u}_d \\ \boldsymbol{u}_o \end{bmatrix} + \phi^2 \begin{bmatrix} Q_{dd} & Q_{do} \\ Q_{od} & Q_{oo} \end{bmatrix} \begin{bmatrix} \boldsymbol{u}_d \\ \boldsymbol{u}_o \end{bmatrix}_+^p = \mathbf{0}. \tag{3.30}$$

Now, since the vector $\boldsymbol{u}_d$ is known, then dimension of matrix equation can be decreased to the number of unknown nodes only. Thus, the desired matrix equation reads as follows

$$M_{od}\dot{\boldsymbol{u}}_d + M_{oo}\dot{\boldsymbol{u}}_o + K_{od}\boldsymbol{u}_d + K_{oo}\boldsymbol{u}_o + \phi^2 Q_{od}(\boldsymbol{u}_d)_+^p + \phi^2 Q_{oo}(\boldsymbol{u}_o)_+^p = \mathbf{0}, \tag{3.31}$$

which can be simplified further

$$M_{oo}\boldsymbol{u}_o + K_{od}\boldsymbol{u}_d + K_{oo}\boldsymbol{u}_o + \phi^2 Q_{od}(\boldsymbol{u}_d)_+^p + \phi^2 Q_{oo}(\boldsymbol{u}_o)_+^p = \mathbf{0} \tag{3.32}$$

due to $\dot{\boldsymbol{u}}_d = \mathbf{0}$. The Crank-Nicolson method is applied to discretize in time the above ODE system. Then, the time-marching scheme for (3.32) reads as follows

$$\begin{aligned} \boldsymbol{u}^{n+1} = \left(\frac{M_{oo}}{\Delta t} + \frac{K_{oo}}{2}\right)^{-1} \Bigg(& - \phi^2 Q_{od}\boldsymbol{u}_d - \phi^2 Q_{oo}\Big(\frac{\boldsymbol{u}^{n+1} + \boldsymbol{u}^n}{2}\Big)_+^p - K_{od}\boldsymbol{u}_d \\ & + \frac{M_{oo}}{\Delta t}\boldsymbol{u}^{n+1} - \frac{K_{oo}}{2}\boldsymbol{u}^n \Bigg). \end{aligned} \tag{3.33}$$

Additionally, in each step we perform the projection step

$$\boldsymbol{u}^{n+1} = 0.5\max(\boldsymbol{u}^{n+1}, 0) + 0.5\max(\boldsymbol{u}^n, 0)\,.$$

to ensure the positivity of the approximate solution. The *MATLAB* code is presented Appendix.

Chapter 4

Numerical results and discussion

4.1 Implementation aspects

In this section the implementation aspects are discussed. The time-marching scheme was implemented in *MATLAB* via PDE Toolbox. Since both models from Chapter 4 are posed over a square domain $\Omega = (0, 1)^2$, we use the same geometry, see Figure 4-1.

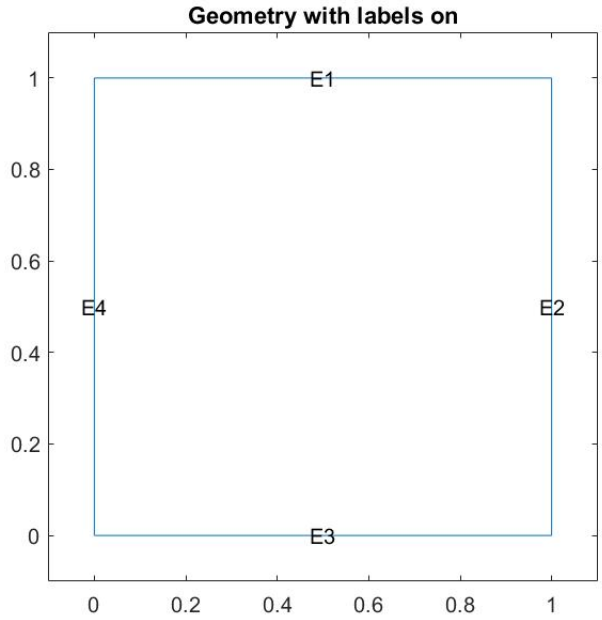

Figure 4-1: Geometry with labels on

The piecewise linear finite elements are used for both models, see the regular triangular mesh shown in Figure 4-2.

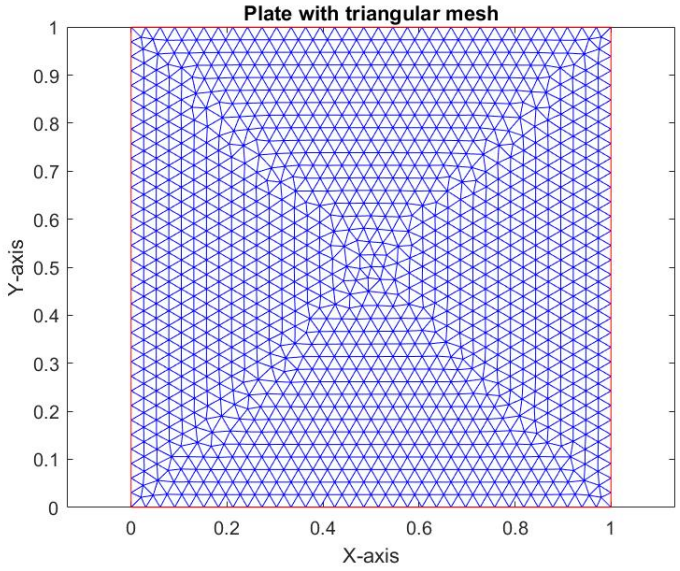

Figure 4-2: Triangular mesh with mesh size $h = 0.03$.

In PDE Toolbox it is also possible to vary the mesh size and display the numbering of nodes, as shown in Figure 4-3. We use this picture in section 4.2 to find out the structure of the solution vector and system matrices.

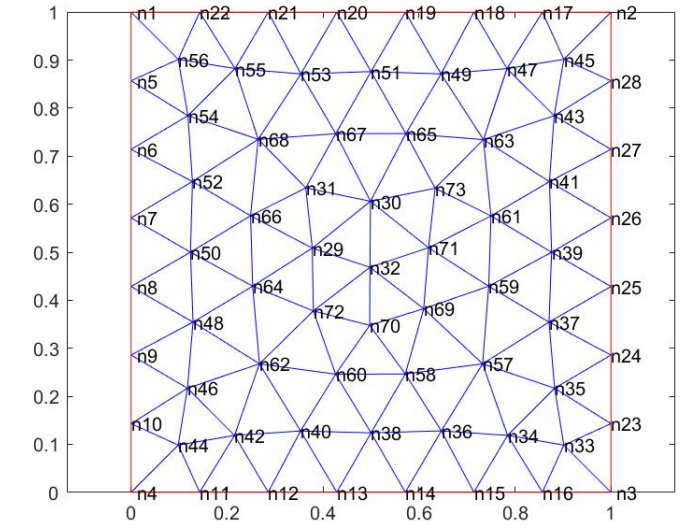

Figure 4-3: Triangular mesh with mesh size $h = 0.15$.

Using *applyBoundaryConditions* it is possible to introduce different boundary conditions, and *assembleFEMatrices* assembles all the finite element matrices. Further, having all the matrices we artificially create solution vectors and use the time-stepping scheme from Chapter 3 to construct the time loop. Formulae for the time-stepping scheme are given in Chapter 3 by equations (3.14) and (3.33).

4.2 Model with volume reaction in catalytic reactor

Numerical solutions of (3.1) are presented in this section. Figures 4-4, 4-5 and 4-6 shows the numerical solution for $p = 0.01$ and $\phi = 6$, $\phi = 8$ and $\phi = 3.5$, respectively. On the boundary we have maximum concentration of a substance, which decreases monotonically towards the center. In the center of the domain we see the dead-core. Since the solution is obtained through finite element approximations, it is important to compare with the exact analytical results.

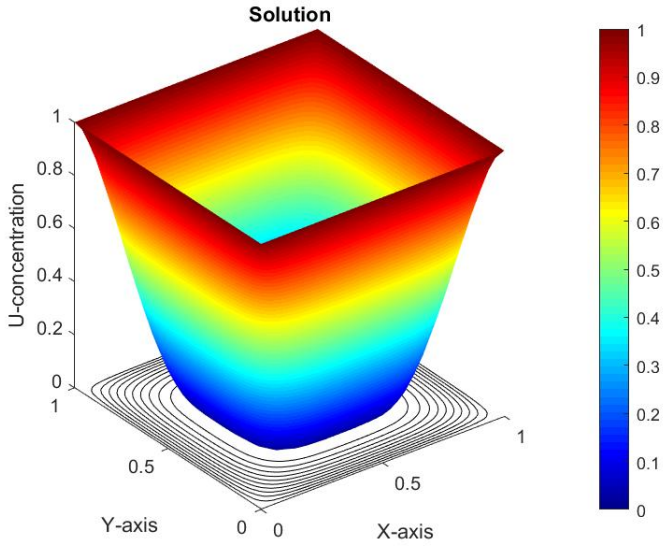

Figure 4-4: Dead-core solution of (3.1) for $p = 0.01, \phi = 6$.

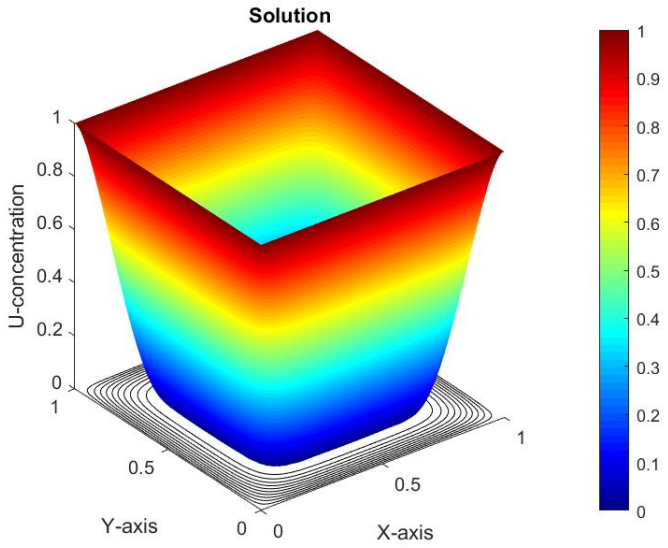

Figure 4-5: Dead-core solution of (3.1) for $p = 0.01, \phi = 8$.

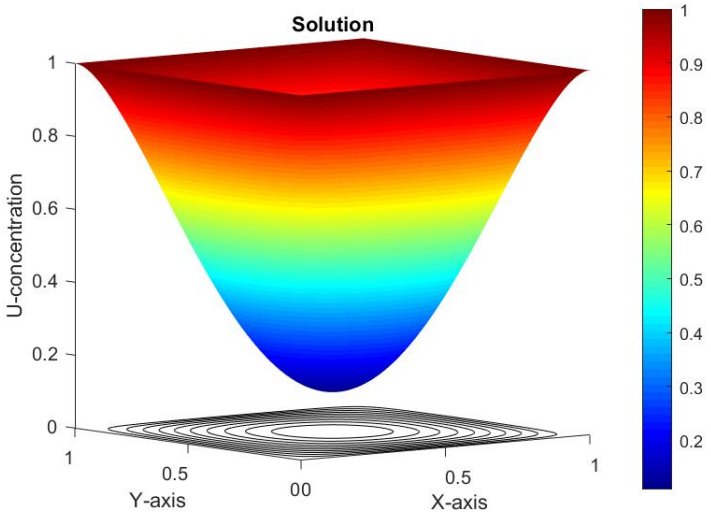

Figure 4-6: Dead-core solution of (3.1) for $p = 0.01, \phi = 3.5$.

In the Figure 4-7 the dead-core boundaries for different values of ϕ for $p = 0.01$ were presented.

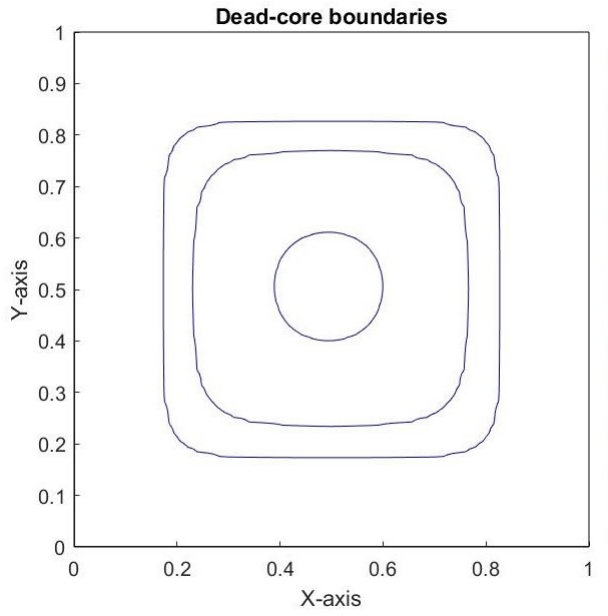

Figure 4-7: Boundaries of dead-core for $p = 0.01$, $\phi = 4, 6, 8$.

The result shown in Figure 4-7 agrees with an intuition that the larger reaction rate coefficient increases the size of the dead-core. As mentioned in the introduction, in [1] Thiele modulus is found, which is a minimum value of ϕ^* for a dead-core.

$$\phi^* = \sqrt{\frac{2}{1-p}\left(\frac{1+p}{1-p} + s\right)}\left\{1 + \frac{2}{Bi_m(1-p)}\right\}^{(p-1)/2}$$

according to the Dirichlet boundary conditions, $Bi_m \to \infty$. Let us check the Thiele modulus for cylindrical shape, which corresponds to $s = 1$. Thus, the above formula is now simplified to

$$\phi^* = \sqrt{\frac{2}{1-p}\Big(\frac{1+p}{1-p} + 1\Big)} = \sqrt{\frac{2}{1-p}\Big(\frac{2}{1-p}\Big)} = \frac{2}{1-p}.$$

In the Figures 4-8 and 4-9 the dead-core boundaries for cylindrical shape are shown. For $p = 0.1$, $p = 0.01$, Thiele moduli are $\phi^* \approx 2.22$ and $\phi^* \approx 2.02$, respectively. Thus, choosing $\phi = 2.23$ and $\phi^* = 2.03$ produces very small dead-cores.

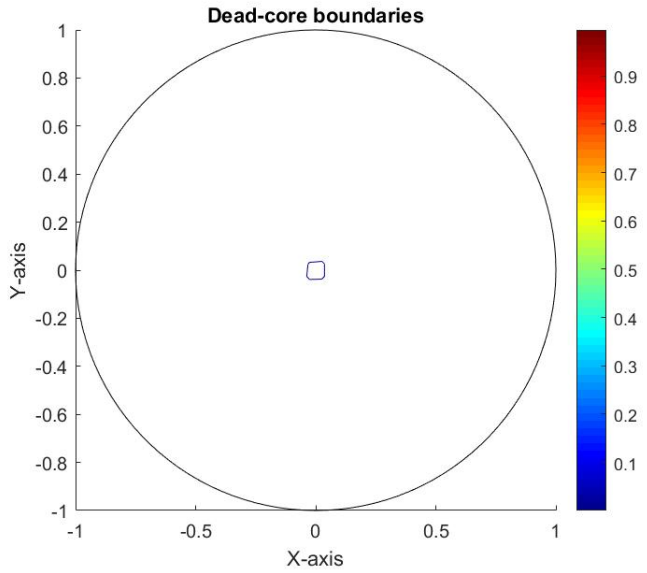

Figure 4-8: Dead-core boundary for $p = 0.1, \phi^* = 2.23$.

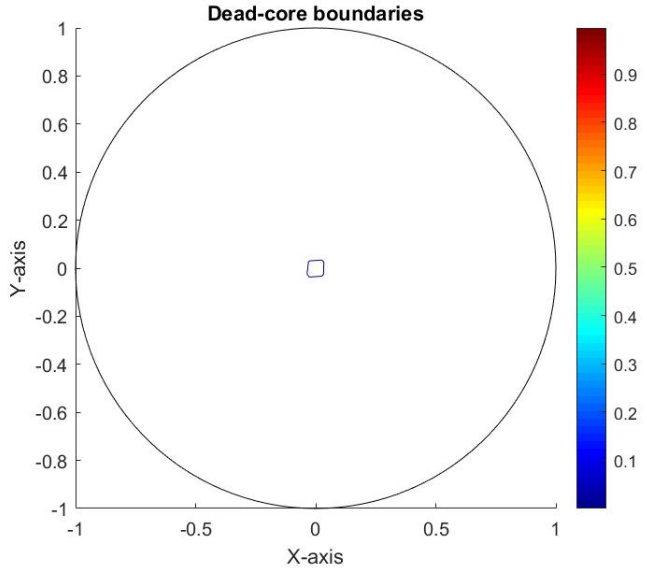

Figure 4-9: Dead-core boundary for $p = 0.01, \phi^* = 2.03$.

Another comparison can be done with analytical results in [18]. The author considered the steady-state case of (3.2). In his work he localized the dead-core and showed the regions where the dead-core should appear for values $p = 0.5$ and $\phi = 15, 30$. Below, Figures 4-10, 4-11 illustrate the dead-cores for $p = 0.5, \phi = 15, 30$. The dead-core

boundaries are marked in blue whereas the regions defined in [18] are with boundaries marked in magenta.

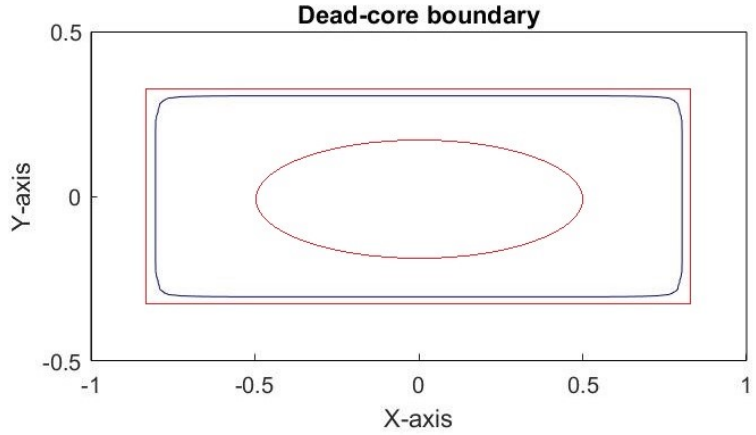

Figure 4-10: Dead-core boundary for $p = 0.5, \phi = 15$.

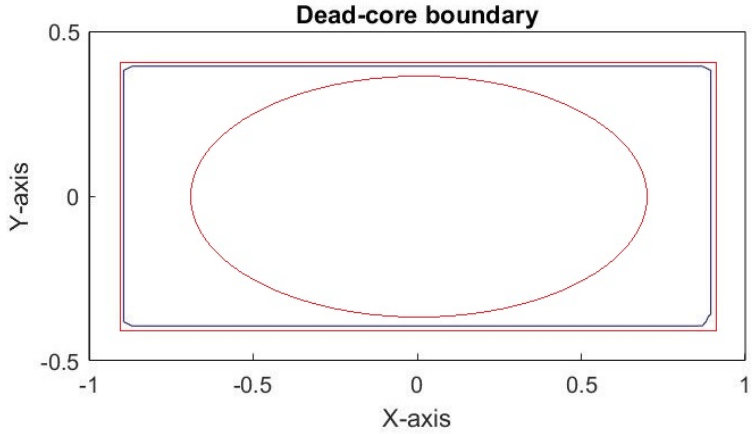

Figure 4-11: Dead-core boundary for $p = 0.5, \phi = 30$.

According to [4] the finite element solution converges to the weak solution in the H^1 semi-norm as mesh size parameter h tends to zero. All the numerical simulations were obtained using the mesh of size $h = 0.01$. Thus, we can conclude that the proposed finite element method works. The presented solutions were obtained by using the proposed time-stepping and product approximation from [5]. Since the profiles in Figures 4-10, 4-11 agree with theoretical predictions in [18], we can state

that the proposed numerical approach works well for the problem (3.2).

4.3 Model for membrane reactor

This section presents results of numerical simulations for the problem of membrane reactor (3.19). In Figure 4-12, 4-14 and 4-15 the numerical solutions are presented for $p = 0.0001$ and $\phi = 1$, $\phi = 2$ and $\phi = 0.8$, respectively. In Figure 4-13 the solution profile along the membrane is shown. The concentration is at maximum on the Dirichlet boundary part and decreases monotonically as x increases forming the dead-core, which begins from approximately $x = 0.8$ and continues until the boundary $x = 1$.

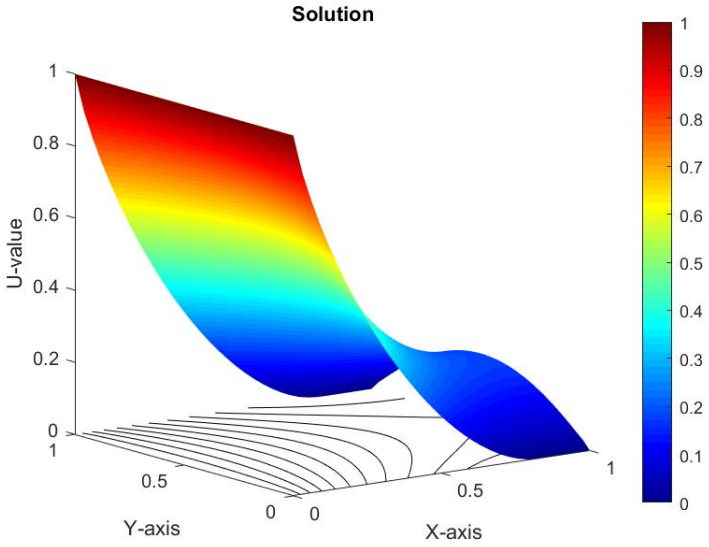

Figure 4-12: Solution with dead-core at the boundary for $p = 0.0001, \phi = 1$.

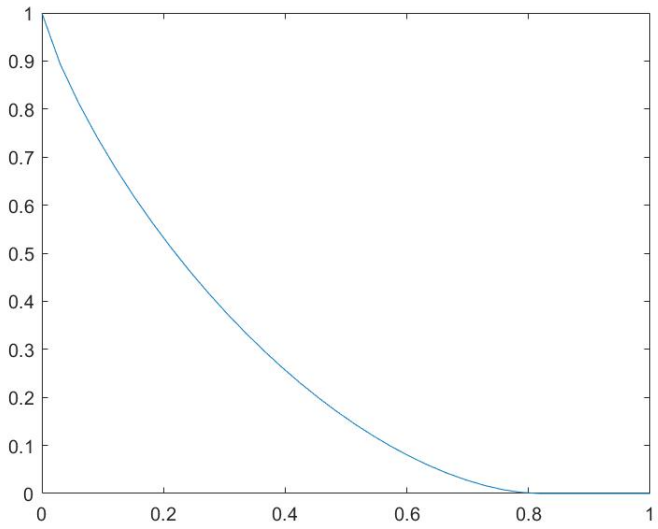

Figure 4-13: Solution profile along the membrane for $p = 0.0001, \phi = 1$.

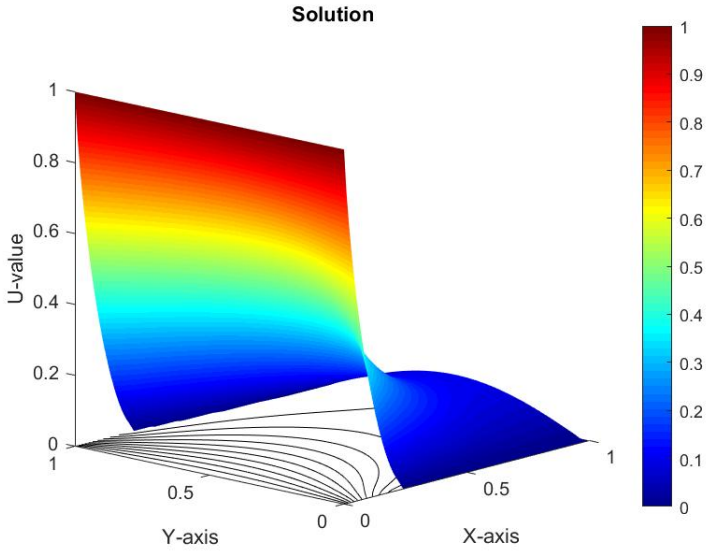

Figure 4-14: Solution with dead-core at the boundary for $p = 0.0001, \phi = 2$.

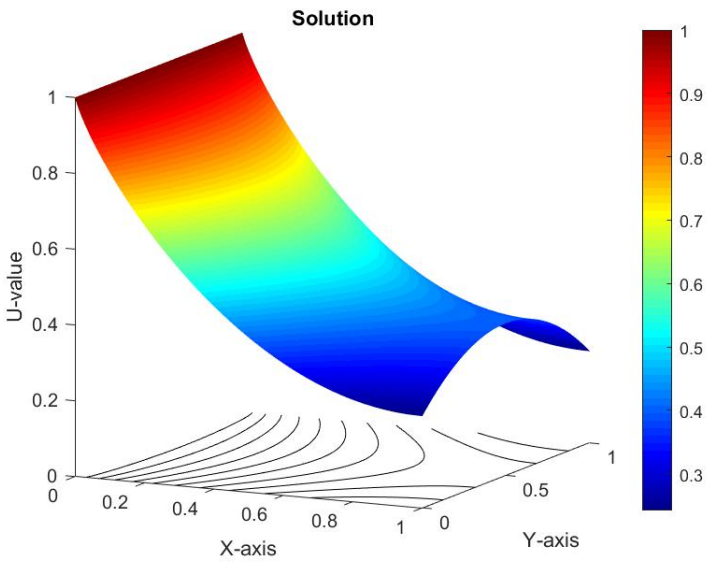

Figure 4-15: Non-dead-core solution for $p = 0.0001, \phi = 0.8$.

In Figure 4-16 the solution profiles along the membrane are presented for the reaction exponent $p = 0.1$ and varying Thiele modulus $\phi = 1, 1.25, 1.5, 1.75, 2$. The behavior of solution agrees with the intuition that increasing reaction rate coefficient increases the size of the dead-core. From physical perspective it can also be justified as follows. The stronger reaction leads to more consumption of the reactant which can result in the bigger dead-core.

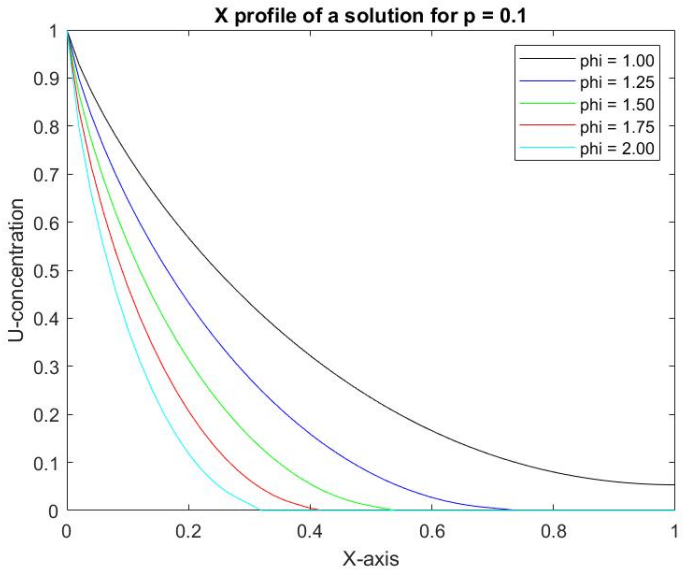

Figure 4-16: Concentration profiles along the membrane for $p = 0.1, \phi = 1, 1.25, 1.5, 1.75, 2$.

In Figure 4-17 the solution profiles along membrane are presented for the Thiele modulus $\phi = 1.25$ and varying reaction exponent $p = 0.2, 0.1, 0.01, 0.0000001$. The effect of decreasing reaction exponent agrees with the physical perspective. Since $0 \leq u \leq 1$, then $[u]_+^p$ increases with decreasing p. However, as we see in Figure 4-17, for small p the change is not very significant. Even though, $p = 0.0000001$ is much less than $p = 0.01$, the increase in the dead-core length is hardly noticeable.

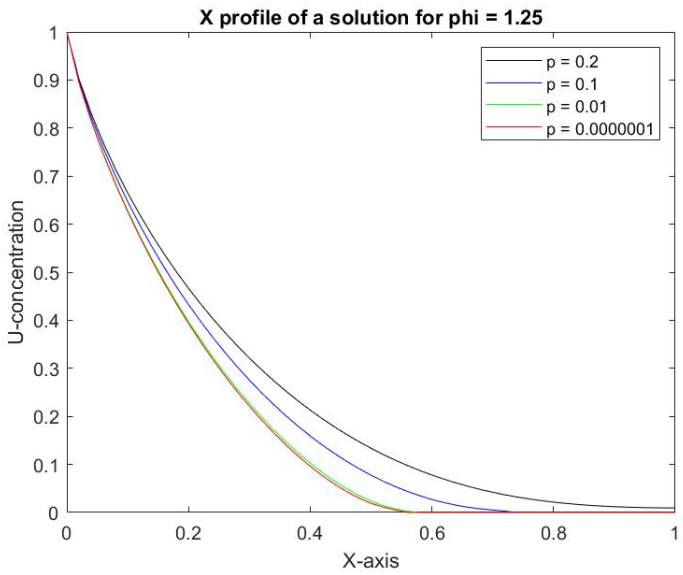

Figure 4-17: Concentration profiles along the membrane for $\phi = 1.25$, $p = 0.2, 0.1, 0.01, 0.0000001$.

The finite element error bounds for (3.19) can be derived by analogy to the case with the volume reaction. However, the approximate solutions agree with physical intuition. The increase in ϕ or decrease in p leads to the increasing size of dead-core. In concluding, the product approximation and time-stepping worked well for the membrane reactor problem (3.19).

Chapter 5

Conclusions

In general, this thesis considered modeling of a dead-core phenomena and looked at the following aspects: influence of parameters p, ϕ on the size of dead-core in different models, and convergence of a time-dependent solution towards the steady-state solution.

For one-dimensional model (2.2) uniqueness of a solution was proved by hand, followed by proofs of boundedness and monotonicity of weak solutions. Another result is Lipschitz continuity with respect to λ for stationary problem with planar geometry (2.3). This lead to a point-wise convergence of a solution for time-dependent problem to a solution for steady-state one.

Two-dimensional model with volume reaction was solved numerically, particularly with Finite Element method using P_1 elements and Group approximation method combined with time-stepping approach. Numerical simulations verified theoretical predictions, thus, the approximation was successful. Solutions clearly showed that increase in ϕ leads to an increase of the dead-core size, while increase in p decreases it. Boundedness of a weak solution was proved for both volume reaction and membrane reactor problems. Membrane reactor problem is an essence of this project and for this model novel results were obtained. Group method approximation with time-stepping method were successfully applied to this problem. Numerical simulations showed that the effect of ϕ and p on the size of a dead-core is similar to the volume reaction problem.

Chapter 6

Appendix

6.1 MATLAB code for reactor with volume reaction

```
% below are coefficients from equation
phi = 7.7; %reaction coefficient
pex = 0.75; %power p
model = createpde;

%below is the geometry itself
rect=[3
     4
     0
     1
     1
     0
     1
     1
     0
     0];
gd = [rect];
```

```
ns = char('rect');
ns = ns';
sf = 'rect';
g = decsg(gd, sf, ns);

%this geometry is for disc-shaped domain
%disc = [1
%     0
%     0
%     1];
%gd = [disc];
%ns = char('disc');
%ns = ns';
%sf = 'disc';
%g = decsg(gd, sf, ns);
geometryFromEdges(model, g);

%Below is the plot of the geometry

figure;
pdegplot(model, 'EdgeLabels', 'on');
axis([-1.1 1.1 -1.1 1.1]);
title 'Geometry with labels on';
applyBoundaryCondition(model,'Edge',1:model.Geometry.NumEdges,'u',1);
f = @(location,state) -phi^2*max(state.u, 0).^pex;
specifyCoefficients(model,'m',0,'d',1,'c',1,'a',0,'f',f);
setInitialConditions(model, 1);
hmax = .05; %element size
msh = generateMesh(model,'Hmax',hmax, 'GeometricOrder', 'linear');
figure;
```

```
pdeplot(model);
axis equal
title 'Plate with triangular mesh'
xlabel 'X-axis'
ylabel 'Y-axis'

FEM = assembleFEMatrices(model)
K = FEM.K;
M = FEM.M;
R = FEM.R;
F = FEM.F;
Ndir = length(R); %number of dirichlet nodes
Nall = length(F); %number of all nodes
Ninner = Nall-Ndir; %number of inner nodes
Kid = K(Ndir+1:Nall, 1:Ndir); %stiffness matrix with Dirichlet and
Inner nodes
Mid = M(Ndir+1:Nall, 1:Ndir); %mass matrix with Dirichlet and
Inner nodes
FEMn = assembleFEMatrices(model, 'nullspace');
Kii = FEMn.Kc; %stiffness matrix with Inner nodes only
Mii = FEMn.M; %mass matrix with Inner nodes only
I = speye(Ninner, Ninner);



%boundary conditions
udir = ones(Ndir, 1); %u on dirichlet nodes
uold = zeros(Ninner, 1); %first guess of u at inner nodes

%Dirichlet nodes value of u
uD = ones(Ndir, 1);
```

```
%dead-core bound
uzeross = 0.0000001*ones(Ndir, 1);

%fixed point interation
unew = zeros(Ninner, 1);
uzero = zeros(Ninner, 1);
uzerodir = zeros(Ndir, 1);
%time stepping
unew_new = zeros(Ninner, 1);
nt = 5000;
deltaT = 1/(nt-1);

%for plotting
ufull = zeros(Nall, 1);
x=linspace(0, 1, Nall);

for i=1:nt
    for j=1:2
        unew = ((1/deltaT)*Mii + 0.5*Kii)\( -Kid*uD - phi^2*Mid*uD
        - 0.5*Kii*uold - phi^2*Mii*max((unew + uold)/2,0).^pex
        + (1/deltaT)*Mii*uold);
        uold = 0.5*max(unew,0) + 0.5*max(uold,0);
    end
    unew_new = max(unew, 0);
    uold = unew_new;
    ufull(1:Ndir) = udir;
    ufull(Ndir+1:Nall) = uold;

end
```

```
figure;
pdeplot(model, 'XYData', ufull,'ZData', ufull, 'Contour', 'on',
'Mesh', 'off', 'Colormap', 'jet');
title 'Solution'
xlabel 'X-axis'
ylabel 'Y-axis'
zlabel 'U-value'

figure;
pdeplot(model, 'XYData', ufull, 'XYStyle', 'off', 'Contour', 'on',
'Levels', uzeross,'Colorbar', 'on', 'Colormap', 'jet');
xlabel 'X-axis'
ylabel 'Y-axis'
title 'Level curve'
```

6.2 MATLAB code for membrane reactor

```
clear all;
phi = 3.0; %reaction coefficient
pex = 0.1; %power p
alpha = 1; %dummy variable for artificial Neumann boundary condition
uzero = 0.1; %dummby variable for artificial Neumann boundary condition
model = createpde;

% the geometry
rect=[3
    4
    0
    1
```

```
    1
    0
    1
    1
    0
    0];
gd = [rect];
ns = char('rect');
ns = ns';
sf = 'rect';
g = decsg(gd, sf, ns);

geometryFromEdges(model, g);
%[p,e,t] = initmesh(gd)
%Below is the plot of the geometry

figure;
pdegplot(model, 'EdgeLabels', 'on');
axis([-0.1 1.1 -0.1 1.1]);
title 'Geometry with labels on';
applyBoundaryCondition(model, 'dirichlet' ,'Edge', 4, 'u', 1);
applyBoundaryCondition(model, 'neumann', 'Edge', 1, 'q', alpha,
'g', uzero);
applyBoundaryCondition(model, 'neumann', 'Edge', 3, 'q', alpha,
'g', uzero);
applyBoundaryCondition(model, 'neumann', 'Edge', 2, 'q', 0, 'g', 0);
specifyCoefficients(model,'m',0,'d',1,'c',1,'a',0,'f',0);
setInitialConditions(model, 1);
hmax = .02; %element size
msh = generateMesh(model,'Hmax',hmax, 'GeometricOrder', 'linear');
```

```
figure;
pdeplot(model);
axis equal
title 'Plate with triangular mesh'
xlabel 'X-axis'
ylabel 'Y-axis'
FEM = assembleFEMatrices(model)
K = FEM.K;
A = FEM.A;
F = FEM.F;
Q = FEM.Q;
G = FEM.G;
H = FEM.H;
R = FEM.R;
M = FEM.M;

% number of Dirichlet nodes, also number of nodes on each Edge of
geometry
Ndir5 = size(R,1);

% last Dirichlet node
Ndirlast = 5 + Ndir5 - 3;

pdemesh(model, 'NodeLabels', 'on');

% the number of the first and last node on reaction wall
[row, col] = find(Q);
Nreactionlast = max(row);
Nreactionfirst = 5 + Ndir5 - 2;
```

```
% the first  and last nodes of zero Neumann
Neumannzerofirst = Nreactionlast + 1;
Neumannzerolast = Neumannzerofirst + Ndir5 - 3;

% taking 2,3 columns to Neumannzero columns
Neulastupd = Neumannzerolast - 2;
vecs_M = M(:, 2:3);
M(:, 2:3) = [];
Mupd1 = [M(:, 1:Neulastupd) vecs_M M(:, Neulastupd+1:end)];

vecs_K = K(:, 2:3);
K(:, 2:3) = [];
Kupd1 = [K(:, 1:Neulastupd) vecs_K K(:, Neulastupd+1:end)];

vecs_Q = Q(:, 2:3);
Q(:, 2:3) = [];
Qupd1 = [Q(:, 1:Neulastupd) vecs_Q Q(:, Neulastupd+1:end)];

% taking 2,3 rows to Neumannzero rows
rows_Mupd1 = Mupd1(2:3, :);
Mupd1(2:3, :) = [];
Mupd2 = [Mupd1(1:Neulastupd, :); rows_Mupd1;
Mupd1(Neulastupd+1:end, :)];

rows_Kupd1 = Kupd1(2:3, :);
Kupd1(2:3, :) = [];
Kupd2 = [Kupd1(1:Neulastupd, :); rows_Kupd1;
Kupd1(Neulastupd+1:end, :)];

rows_Qupd1 = Qupd1(2:3, :);
```

```
Qupd1(2:3, :) = [];
Qupd2 = [Qupd1(1:Neulastupd, :); rows_Qupd1;
Qupd1(Neulastupd+1:end, :)];

%dividing solution vector u to dirichlet and unknown parts
Nall = length(M);
Nother = Nall - (Ndirlast - 2);

u = ones(Nall, 1);
ud = u(1:Ndirlast-2, 1);
uo = u(Ndirlast-1:end, 1);
uo = zeros(Nother, 1);

%dividing matrices M, K, Q to dirichlet and other parts
Kdd = Kupd2(1:Ndirlast-2, 1:Ndirlast-2);
Kdo = Kupd2(1:Ndirlast-2, Ndirlast-1:end);
Kod = Kupd2(Ndirlast-1:end, 1:Ndirlast-2);
Koo = Kupd2(Ndirlast-1:end, Ndirlast-1:end);

Mdd = Mupd2(1:Ndirlast-2, 1:Ndirlast-2);
Mdo = Mupd2(1:Ndirlast-2, Ndirlast-1:end);
Mod = Mupd2(Ndirlast-1:end, 1:Ndirlast-2);
Moo = Mupd2(Ndirlast-1:end, Ndirlast-1:end);

Qdd = Qupd2(1:Ndirlast-2, 1:Ndirlast-2);
Qdo = Qupd2(1:Ndirlast-2, Ndirlast-1:end);
Qod = Qupd2(Ndirlast-1:end, 1:Ndirlast-2);
Qoo = Qupd2(Ndirlast-1:end, Ndirlast-1:end);

%fixed point iteration
```

```
unew = zeros(Nother, 1);
uold = zeros(Nother, 1);
%time stepping
unew_new = zeros(Nother, 1);
nt = 5000;
deltaT = 1/(nt-1);
ufull = zeros(Nall, 1);

%loop

for i=1:nt
    for j=1:2
        unew = ((1/deltaT)*Moo + 0.5*Koo)\(-phi^2*Qod*ud
        - phi^2*Qoo*max((unew + uold)/2,0).^pex - Kod*ud
        + (1/deltaT)*Moo*uold - 0.5*Koo*uold);
        uold = 0.5*max(unew, 0) + 0.5*max(uold, 0);
    end
    unew_new = max(unew, 0);
    uold = unew_new;
    ufull(1:Ndirlast-2) = ud;
    ufull(Ndirlast-1:Nall) = uold;
end

%now we are putting rows 2,3 back to its original places
nodes_23 = ufull(Neulastupd+1:Neulastupd+2);
ufull(Neulastupd+1:Neulastupd+2) = [];
ulast = [ufull(1); nodes_23; ufull(2:end)];

figure;
pdeplot(model, 'XYData', ulast,'ZData', ulast, 'Contour', 'on',
```

```
'Mesh', 'off', 'Colormap', 'jet');
title 'Solution'
xlabel 'X-axis'
ylabel 'Y-axis'
zlabel 'U-value'

%the code below is to assemble the solution when y=0,
%so we are looking only at x-axis
Nreactionmid = Nreactionfirst + (Ndir5 - 3);
Nreactionmidnumber = 3 + Nreactionmid - Nreactionfirst;
x=linspace(0, 1, Nreactionmidnumber);
ureaction = [ulast(4); ulast(Nreactionfirst:Nreactionmid); ulast(3)];
figure;
plot(x, ureaction);
```

Bibliography

[1] Vsevolod V. Andreev. Formation of a "dead zone" in porous structures during processes that proceeding under steady-state and unsteady-state conditions. *Review Journal of Chemistry*, 3(3):239–269, 2013.

[2] A.K. Aziz, A.B. Stephens, and Manil Suri. Numerical methods for reaction-diffusion problems with non-differentiable kinetics. *Numerische Mathematik*, 53(1-2):1–11, 1988.

[3] C. Bandle, R.P. Sperb, and I. Stakgold. Diffusion and reaction with monotone kinetics. *Nonlinear Analysis: Theory, Methods & Applications*, 8(4):321 – 333, 1984.

[4] John W. Barrett and Robert M. Shanahan. Finite element approximation of a model reaction-diffusion problem with a non-Lipschitz nonlinearity. *Numerische Mathematik*, 59(1):217–242, 1991.

[5] Ian Christie, David F. Griffiths, Ronald Mitchell, and Jesús Marıa Sanz-Serna. Product approximation for non-linear problems in the finite element method. *IMA Journal of Numerical Analysis*, 1(3):253–266, 1981.

[6] Guowei Dai, Ruyun Ma, Haiyan Wang, Feng Wang, and Kuai Xu. Partial differential equations with robin boundary condition in online social networks. *Discrete & Continuous Dynamical Systems-B*, 20(6):1609, 2015.

[7] Lawrence C. Evans. Partial differential equations. *Graduate studies in mathematics*, 19(2), 1998.

[8] Herbert Gajewski, Konrad Gröger, and Klaus Zacharias. Nichtlineare operatorgleichungen und operator-differentialgleichungen. *Mathematische Nachrichten*, 67(22):iv–iv, 1975.

[9] B. Golman, K. Shinohara, and M. Kobayashi. Selectivity and yield of exothermic consecutive reactions in catalytically active porous membrane reactor. *Journal of chemical engineering of Japan*, 30(3):507–513, 1997.

[10] P. Knabner and L. Angerman. *Numerical Methods for Elliptic and Parabolic Partial Differential Equations*. Texts in Applied Mathematics. Springer New York, 2006.

[11] Tiberiu M. Leib and Carmo Joseph Pereira. *Perry's Chemical Engineers' Handbook: Reactors*. McGraw-Hill, 2008.

[12] C.V. Pao. *Nonlinear Parabolic and Elliptic Equations*. Fems Symposium. Springer US, 1992.

[13] Riccardo Ricci. Large time behavior of the solution of the heat equation with nonlinear strong absorption. *Journal of Differential Equations*, 79(1):1 – 13, 1989.

[14] F. Sabit. Capstone project: Analysis of dead core phenomena in reaction-diffusion problems. `https://nur.nu.edu.kz/handle/123456789/4678`, 2020.

[15] F. Sabit, M. Shakipov, P. Skrzypacz, and B. Golman. Dead-core solutions to simple catalytic reaction problems in chemical engineering. *Eurasian Chemico-Technological Journal*, 21(1):29–33, 2019.

[16] Piotr Skrzypacz, Vsevolod V. Andreev, and Boris Golman. Dead-core and non-dead-core solutions to diffusion-reaction problems for catalyst pellets with external mass transfer. *Chemical Engineering Journal*, 385:123927, 2020.

[17] A. Spence, D.J. Worth, and S.T. Kolaczkowski. The treatment of non-integer exponents in reaction rate expressions. *Computers & Chemical Engineering*, 19(11):1169–1171, 1995.

[18] R.P. Sperb. Some complementary estimates in the dead core problem. In *Research Report/Seminar für Angewandte Mathematik*, number 09. Eidgenössische Technische Hochschule, Seminar für Angewandte Mathematik, 1995.

[19] M. Szukiewicz, E. Chmiel-Szukiewicz, K. Kaczmarski, and A. Szałek. Dead zone for hydrogenation of propylene reaction carried out on commercial catalyst pellets. *Open Chemistry*, 17(1):295–301, 2019.